JOURNAL OF MATERIALS SCIENCE 18 (1983) 321–347

Review
Storing energy in metal hydrides: a review of the physical metallurgy

DOUGLAS G. IVEY, DEREK O. NORTHWOOD
Department of Engineering Materials, University of Windsor, Windsor, Ontario, Canada N9B 3P4

Metal hydrides, as energy storage media, are receiving considerable attention. The amount of literature concerning the properties of these materials has increased markedly over the past few years. In this paper, we conduct a review of the alloy groups which absorb large quantities of hydrogen. These alloy classes are designated as AB_5, AB, AB_2, AB_3 and A_2B_7 and Mg-based compounds. These materials are discussed with emphasis placed on thermodynamic and kinetic properties, activation and deactivation, poisoning effects and storage capacity.

1. Introduction

With the rapidly diminishing non-renewable energy supplies and greater environmental awareness comes the need for more efficient and cleaner-running fuels. Hydrogen may be able to provide a solution. Hydrogen is a promising medium for both energy transmission and storage. It is essentially non-polluting, the major by-product of combustion being H_2O, and it can be generated from readily available and abundant raw materials and energy sources. Hydrogen has the highest energy density per unit weight of any chemical and has a diversified number of uses, ranging from internal combustion engines to fuel cells. One of the greatest limitations surrounding the exploitation of hydrogen as a fuel, however, appears to be the difficulty in storing it economically and conveniently.

Hydrogen can be extracted from fossil fuels, from water, or both [1–5]. Fossil fuels are a limited and diminishing resource but water can be considered inexhaustible. In addition to the raw materials (coal, water, etc.) energy must be utilized to extract the hydrogen. This energy can be derived from primary energy sources such as hydro-electricity, nuclear, solar, wind, fossil, geothermal, or ocean temperature gradients.

If hydrogen is to be used as a fuel, economical processes for splitting water into hydrogen and oxygen are necessary. Electrolysis of water [1–4] and the thermo-mechanical processes [4] are two methods. Electrolysing water with off-peak electricity does not appear to be too practical in the near future because of the high capital costs and the low round-trip efficiency for the conversion of electricity to hydrogen and back to electricity (35%) [4]. Thermo-mechanical processes utilize heat instead of work to produce hydrogen. This method is only in the experimental stage, but theoretical thermal efficiencies are in the 20 to 50% range [4]. A short-to-medium range method of hydrogen production is from coal [1, 4]. The major problem here, is an environmental one, i.e., the high sulphur content of coal. A summary of various hydrogen production methods is given in Fig. 1.

Hydrogen can be utilized in a number of ways. The most common methods are the combustion of hydrogen in an internal combustion engine [6] and combining hydrogen with oxygen in a fuel cell to produce electricity [7, 8]. Both of these methods have been applied to automobiles and buses in the United States and Europe with limited success. Other methods of utilization involve thermal engines [9], air-conditioning systems [10], and heat exchangers [11].

0022–2461/83/020321–27$05.74/0

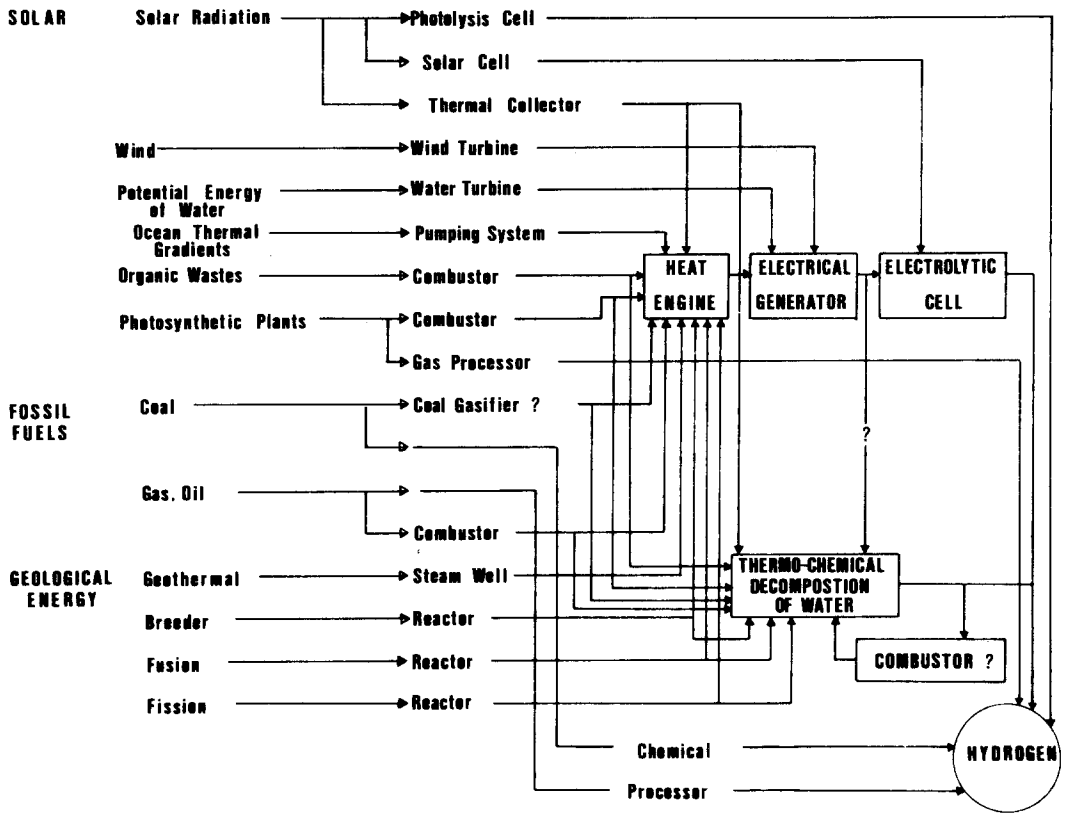

Figure 1 Summary of methods for hydrogen production [4].

The major methods for storing hydrogen are liquid storage, glass microspheres, or metal hydrides. Liquid hydrogen is stored in a Dewar flask [12, 13], which is an insulated container, and the major cost is liquefaction. For a refrigeration cycle that is 33% efficient, the energy for liquefaction is estimated at $10\,kWh\,kg^{-1}$, which is 25% of the heat available from combustion of the hydrogen. Microspheres are small glass spheres of 6 to 60 μm diameter made from fly ash. These spheres are permeable to hydrogen at high temperatures and impermeable at low temperatures. Most of the expense, here, is due to the refilling stage where the hydrogen must be compressed and the system heated to 300° C. The energy required for this process is estimated at 3% of the energy available during combustion. Metal hydrides are chemical compounds of metals and hydrogen. The hydrogen is stored safely inside the metal itself and the amount of hydrogen stored per volume is greater than either gaseous or liquid storage. The major difficulties, at the present time, lie in the weight and cost of the hydriding materials.

The purpose of this paper is to review the properties of metal hydrides and relate these to the requirements for hydrogen storage. The major metal–hydrogen systems will be discussed in terms of hydrogen capacity, thermodynamics, kinetics, surface properties, and contamination, exploring the benefits and problems of each.

2. Bonding and electronic factors of metal hydrides

Hydrogen reacts with metals to form three kinds of metal hydrides, namely saline or ionic, metallic and covalent [14, 15]. The ionic-type bond is made up of metal cations and hydrogen anions. These hydrides are formed by the direct reactions of hydrogen with alkali or alkaline earth metals. Also included in this group is magnesium which demonstrates some covalency. The alkali metal hydrides have a sodium chloride type structure, while the alkaline rare earth hydrides have a barium chloride structure. In general, these hydrides are too stable for hydrogen storage application, with the exception of magnesium. Covalent hydrides are made up of Be and many of the B group metals of the Periodic Table, see Fig. 2. The hydrides may be solid, liquid, or gaseous and can be quite unstable. None of these

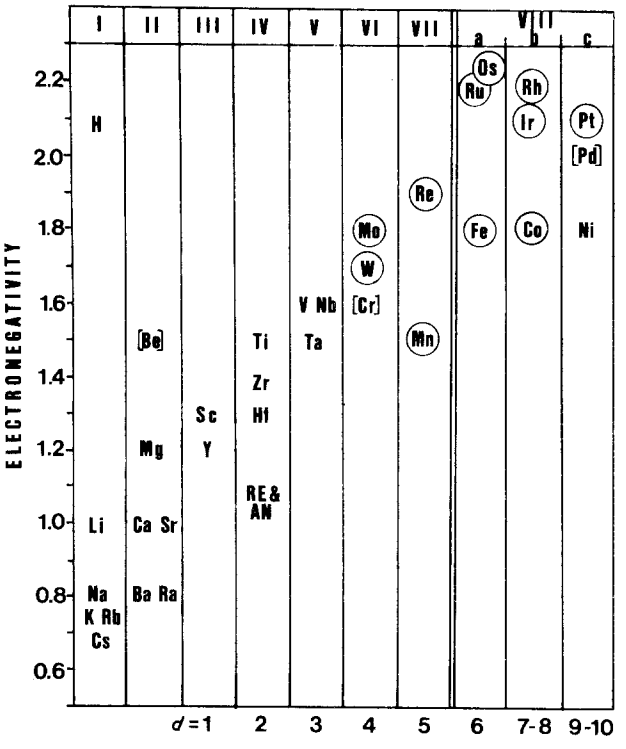

Figure 2 Electronegativities of the transition metals, the rare earths (RE) and the actinides related to that of hydrogen [19].

hydrides are formed by reacting directly with the metal, which eliminates them for storage applications. The type of bonding that is exhibited by the majority of potential hydrogen storage hydrides is metallic in nature. Metallic hydrides have a metallic appearance and high thermal and electrical conductivities. They are formed by the reaction of hydrogen with most of the elements of groups IIIA–VIIIA in the Periodic Table (Fig. 2). The metallic bond in the past has been explained by an anionic or protonic model. These models have practically vanished with the work done in recent years [17, 18] on bond structure.

There are a number of general observations that can be made concerning metallic hydrides [19]:

(1) the metal atoms in metallic hydrides are at least trivalent. Orbital overlap necessitates that there be close metal–metal spacing and entering hydrogen should be considered to be metallic;

(2) the majority of catalytic properties of transition metal and rare earth hydride systems can be explained in terms of d-electron interaction;

(3) most of the properties of the actinide systems (up to plutonium) can be explained in terms of f-electron interactions.

(4) if the d- (or f-) electrons are tied up in metallic bonding, they will not, in general, be readily available for chemisorption-catalysis. Conversely, if the d- (or f-) electrons are not involved in metallic bonding, they will, in general, be available for chemisorption-catalysis.

The type of metals making up the metallic bonds can be divided into three groups, that is the highly electropositive metals, the "less electropositive" metals, and the "still less electropositive" metals [19].

The highly electropositive metals consist of the actinides, the rare earths, and the early transition metals. The basic properties are as follows:

(1) the difference in electronegativities (Δn) between these metals and hydrogen lie in the range 0.5 to 1.0 (see Fig. 3);

(2) the heats of reaction and solution are exothermic;

(3) hydrogen atoms are found in tetrahedral positions;

(4) hydriding reactions tend to be poisoned by electrophilic (electron seeking) molecules.

The "less electropositive" metals are made up of metals such as iron, cobalt, tungsten, etc., and exhibit these properties:

(1) hydrides are not formed easily because of high valences, large cohesive energies, and lattices that are too small;

(2) the difference in electronegativities (Δn) is in the range 0.5 to 0.2;

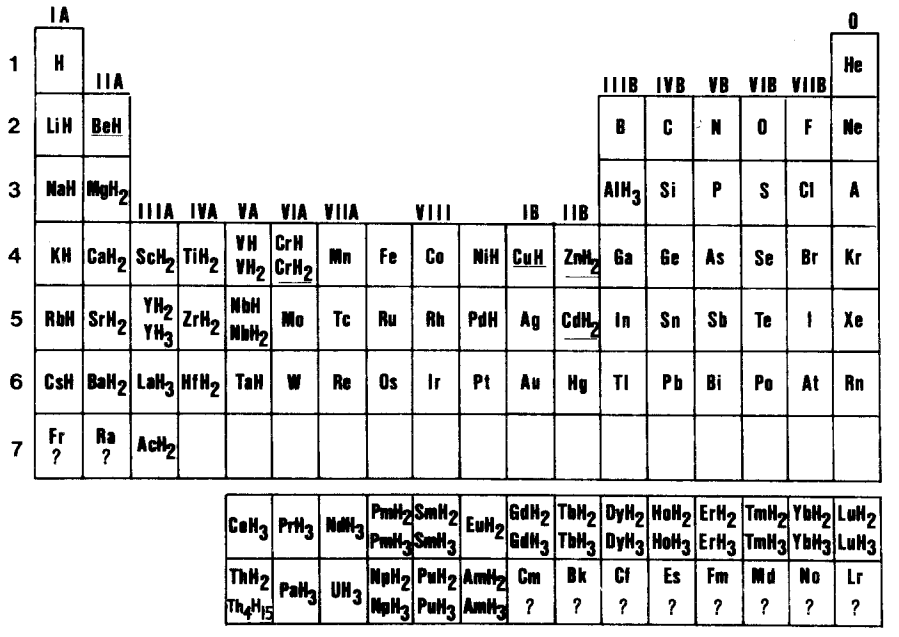

Figure 3 Periodic Table showing occurrence of binary hydrides. The underlined compounds cannot be prepared by a direct reaction [16].

(3) heats of solution become endothermic;

(4) they may cause major electronic effects as alloy additions.

The "still less electropositive" metals include such metals as nickel and palladium. These metals are characterized as follows:

(1) they form hydrides in a complex manner by adding electrons both to the nearly filled metal d-states and also to the new state drawn below the Fermi level;

(2) heats of solution and reaction are complex;

(3) hydrogen atoms are found in octahedral positions;

(4) hydriding reactions tend to be poisoned by electrophobic (electron donating) molecules.

A plot of the electronegativities is shown in Fig. 3. The circled metals do not form hydrides while those in brackets can be forced into unstable hydriding configuration. The differences between the electronegativities, Δn, of hydrogen and a particular metal may be viewed as a driving force or potential for reaction.

Electronic processes in or near the valence-band region can produce large chemical and structural effects [19]. The presence of oxide (and/or hydroxide) films, inclusions, grain-boundary impurities, etc., may be of major importance in dealing with catalytic properties. In the case of the electropositive metals, it appears that hydride initiation (and poisoning) may occur at such sites, rather than directly on the metals. A summary of hydriding properties is given in Table I.

In terms of electrons for chemisorption for extremely pure samples of those metals in which the d-electrons (e.g., Ti and Zr) or f-electrons (e.g., α-U, α-Np, and α-Pa) are almost totally involved in metallic bonding, hydriding is very difficult to initiate. Hydrogen, however, dissociates on the late transition metals almost without an energy of activation. A palladium or nickel

TABLE I Summary of hydriding behaviour of metallic hydride systems [19]

Observation	Electropositive metals	Electronegative metals
Hydride location	Tetrahedral sites	Octahedral sites
Electrical conductivity	Increases upon hydriding	Decreases upon hydriding
Activation energy for dissociation	Appreciable	Nil
Poisoned by	Electrophilic molecules (e.g., SO_2, CO_2 and HCl)	Electrophobic molecules (e.g., NH_3 and pyridine)
Hydride	Is autocatalytic	Poisons reaction

flashing or coating over a more electropositive metal may provide an immediate source of dissociated hydrogen and therefore rapid attack. Electrophobic molecules can poison this dissociation by giving electronic charge to the metal levels that would be ordinarily available.

3. Thermodynamics and kinetics of metal hydrides

Hydrogen reacts reversibly with the metal by means of the following reaction:

$$M + \frac{x}{2} H_2 \rightleftarrows MH_x. \qquad (1)$$

The forward reaction is generally quite exothermic, the heat of formation approaching the heat of combustion of hydrogen in some compounds. The direction of Equation 1 depends on the hydrogen pressure in the system.

The behaviour of metal–hydride systems can be best represented by a pressure, composition, temperature, (P–C–T) diagram. It is a plot of pressure or composition at various temperatures as shown in Fig. 4 [16]. The initial steep slope corresponds to hydrogen going into solid solution and this single-phase region is usually denoted as the α-phase. The position where the curve begins to change slope on the P–C–T diagram denotes the appearance of a metal hydride or β-phase. The solubility of hydrogen in many metals can be quite high, which results in many metal hydrides that are non-stoichiometric. With the formation of the second phase, the hydrogen pressure remains constant and a "plateau" results, as more hydrogen is added. The concentration of hydrogen in each phase does not change, only the relative amounts of each phase. The plateau continues as long as there are two distinct phases, as required by Gibbs' phase rule [20, 21]:

$$F = C - P + 2$$

where P is the number of phases, C is the number of components, and F is the degrees of freedom.

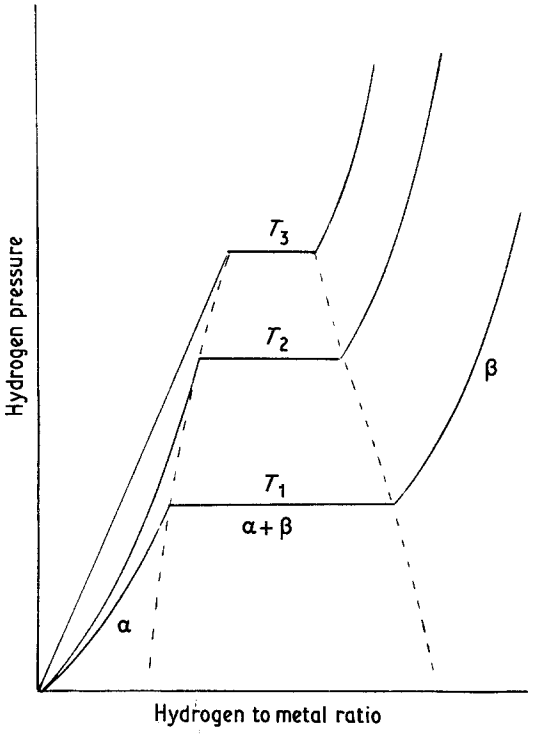

Figure 4 Pressure–composition isotherm showing the relationship between the equilibrium hydrogen pressure and the hydrogen concentration [16].

The effect of temperature is demonstrated in Fig. 4. In general, as the temperature is increased, the miscibility gap tends to narrow, evident in the smaller plateau length. At some critical temperature, the miscibility gap disappears and the α-phase converts continuously into the β-phase. An additional hydride phase, the γ-phase, may also be formed, in which case a second and higher plateau will appear.

The thermodynamics for the formation of a metal hydride can be derived from the van't Hoff isobar [16]:

$$\frac{d \ln K}{dT} = \frac{\Delta H}{RT^2}$$

where R is the gas constant, T is the temperature and ΔH is the heat of reaction.

The equilibrium constant K is given by:

$$K = \frac{a_{MH_x}}{a_M f_{H_2}^{x/2}}.$$

In this equation, the activities (a) can be considered to be ~ 1, since we are working with essentially pure phases. The fugacity (f), because of low pressures, is equivalent to the pressure. Assuming ΔH to be constant (over a relatively small temperature range), the van't Hoff isobar can be written as:

$$d \ln (P_{H_2}^{-x/2}) = \frac{\Delta H}{RT^2} dT,$$

or

$$\ln P_{H_2} = \frac{2}{x} \frac{\Delta H}{RT} + C, \qquad (2)$$

where C is the constant of integration. If the

hydride is stoichiometric and the solubility of hydrogen is small in the α-phase, the heat of formation can be determined from the slope of a plot of $\ln P_{H_2}$ against $1/T$.

The free energy change can be determined by the standard relation:

$$\Delta G = \Delta G_f^\circ + RT \ln K$$

where ΔG_f° is the standard free energy change. At equilibrium, $\Delta G = 0$, which implies that:

$$\Delta G_f^\circ = -RT \ln K$$

or,

$$\Delta G_f^\circ = \frac{x}{2} RT \ln P_{H_2}. \quad (3)$$

The standard entropy of formation can be determined by:

$$\Delta S_f^\circ = \frac{\Delta H_f^\circ - \Delta G_f^\circ}{T}, \quad (4)$$

where ΔH_f° is the standard enthalpy of formation.

In systems that are appreciably non-stoichiometric, the standard enthalpy of formation is the sum of three components: the integral heat of solution of hydrogen in the α-phase from zero hydrogen content to saturation, the heat of reaction in going from the hydrogen-saturated α-phase to the non-stoichiometric β-phase, and the integral heat of solution of hydrogen in the hydrogen-poor β-phase to the stoichiometric value. This also holds for ΔG_f° and ΔS_f°. In cases where there are large deviations from stoichiometry, the thermodynamic quantities are usually expressed as relative partial molal quantities $(\bar{X}_H - 0.5 X_{H_2}^\circ)$, where $\bar{X}_H$ is the partial molal enthalpy (or entropy or free energy) of hydrogen atoms in the solid and $X_{H_2}^\circ$ refers to hydrogen in its standard state as a pure diatomic ideal gas. To obtain the integral quantities, the partial values are integrated over the entire composition from the pure metal to the stoichiometric hydride [16].

Miedema and co-workers [22, 23] have developed a model regarding the formation and dissociation of metal hydrides. The assumptions entering in and the implications coming out of this model are stated as:

(a) the energy effects in alloys of two transition metals, and alloys of transition metals with noble or alkali metals, are mainly nearest-neighbour effects;

(b) the stability of a hydride can be expressed as a function of ΔH alone. The criterion for a hydride to be stable with an equilibrium pressure at room temperature below 1 atm is:

$$H = TS\,(H_2 \text{ gas}) \sim -9 \text{ kcal}^*(\text{mol } H_2)^{-1};$$

(c) intermetallics, that can absorb large quantities of hydrogen near room temperature, have at least one metallic element that can form stable binary hydrides. Examples are Sc, Y, La, Ti, Zr, Hf, Th, U, Pu;

(d) The heat of formation of a ternary hydride, AB_nH_{2m}, from the binary intermetallic AB_n and gaseous H_2 can be resolved into:

$$\Delta H(AB_nH_{2m}) = \Delta H(AH_m) + \Delta H(B_nH_m) - \Delta H(AB_n). \quad (5)$$

For the ternary hydride to be stable at room temperature, with a pressure of 1 atm, the heat of formation has to be more negative than $-9 \text{ kcal}\,(\text{mol } H_2)^{-1}$.

A schematic representation for ternary hydrides [22] is shown in Fig. 5. Metal A is the minority metal in the compound AB_n and attracts hydrogen (hydrides of A are more stable than those of B). The hydrogen atoms primarily surround the A metal atoms. There are contacts between the A atoms and the hydrogen and likewise contacts between the B atoms and hydrogen,

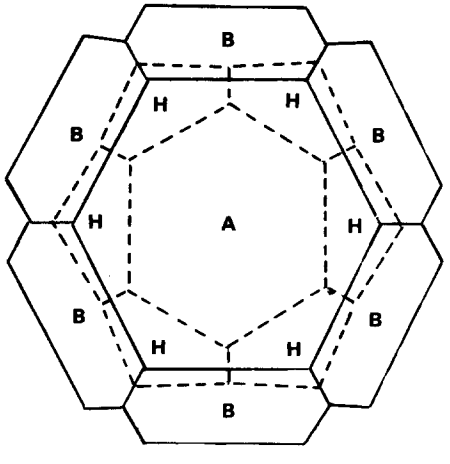

Figure 5 Atomic cells in an intermetallic compound of two metals, A and B, with and without hydrogen present. The atomic cells of hydrogen are indicated by broken lines. Upon hydrogen absorption the lattice is increased, which is not shown here [22].

*1 cal = 4.184 J.

while the atomic contact between A and B, that was responsible for the heat of formation of the original compound, is lost. The contact surface area is approximately the same for A–H and B–H, thereby implying that the ternary hydride, AB_nH_{2m}, is energetically equivalent to a mechanical mixture of AH_m and B_nH_m, so that the heat of formation is given by Equation 5.

It seems that the negative component of Equation 5 has the greatest effect and leads to the rule of reversed stability [22]. This rule states that the more stable the binary intermetallic compounds one starts with, the less will be the tendency to form stable hydrides. There will only be the formation of a stable ternary hydride if at least one of the metals (A) forms fairly stable binary hydrides. For this reason, A is restricted to Sc, Y, Ti, Zr, Hf, Th, U, or Ti.

In metal hydrogen systems, the configurational entropy (ΔS) is relatively constant [22–24] and is equal to $-30.0 \pm 6\,\mathrm{cal\,deg^{-1}(mol\,H_2)^{-1}}$. This entropy effect is predominantly due to the high entropy of hydrogen as a gas, ($31.0\,\mathrm{cal\,deg^{-1}(mol\,H_2)^{-1}}$ at room temperature), which is lost upon entering the metal. Because of the relative constant value of ΔS, the enthalpy value is usually considered the more important value. However, Gruen and Mendelsohn [24] show that entropy changes in a number of AB–H systems differ by up to $6.5\,\mathrm{e.u.(mol\,H_2)^{-1}}$ leading to differences of about $2\,\mathrm{kcal\,(mol\,H_2)^{-1}}$ in the free energies of reactions at 300 K. This corresponds to changes of more than one order of magnitude in hydrogen dissociation pressures.

The reaction kinetics of hydrogen absorption and desorption in metal–hydrogen systems is an important consideration in selecting materials for practical storage applications. Kinetics are hard to follow quantitatively because many hydriding reactions have rate constants of the order of a few seconds. Usual methods cannot follow such rapid changes. A temperature change of a few degrees Celsius is sufficient to alter the kinetics significantly.

The "plateau" behaviour exhibited by hydride systems is similar to many of the phase transformations of the nucleation and growth type [25].

$$F(t) = 1 - \exp\{-(t/\tau)^n\}, \qquad (6)$$

where $F(t)$ is the fraction of reaction completed at time t, τ is the reaction rate time constant (relaxation time), and n is an integer or half-integer, the value of which is governed by the geometries associated with the rate-controlling process. For the $\alpha \rightarrow \beta$ transformation, the fraction of the reaction completed is given by:

$$F(t) = \frac{W(t) - W_\alpha}{W_\beta - W_\alpha} \qquad (7)$$

where $W(t)$ is the weight of absorbed hydrogen at time t, W_α is the weight of absorbed hydrogen in the α-phase limit and W_β is the weight of absorbed hydrogen in the β-phase hydride. Problems are usually encountered in relating these theoretical equations to the actual cases. This is due to the fact that most experimental P–C–T diagrams do not exhibit flat, horizontal plateaus. The slope in the plateau indicates that different portions of the hydride material hydride at different pressures [25]. Impurities, inhomogeneities, particle size and stresses could all be factors contributing to this phenomenon.

The majority of work done on hydriding/dehydriding kinetics to date has been qualitative in nature. The kinetics vary depending upon the material in question. Kinetic, as well as thermodynamic properties, can be affected by alloy composition and crystal structure. Poisoning effects must also be considered, as contaminants may affect the rate-controlling processes. Kinetics is also directly dependent upon the system pressure [26]. The greater the difference between system pressure and equilibrium pressure the faster the reaction rates.

Kinetics can vary from very fast absorption/desorption rates in alloys such as $LaNi_5$, where the reaction rate is controlled by heat transfer [27] to extremely sluggish rates in Mg-alloys, which can be governed by dissociative chemisorption and associative desorption [28]. Kinetics will be discussed in greater detail when each individual alloy system is considered.

4. Hysteresis

In many metal–hydrogen systems, hysteresis has been found. This phenomenon occurs when the transition pressure in a P–C–T curve is higher for absorption than for desorption. An example of hysteresis is shown in Fig. 6. The cause of hysteresis is not fully understood; however, lattice expansion on hydriding is believed to be of importance [29, 30]. The hydride phase seems to cause an irreversible plastic deformation in the matrix. Desorption of a small amount of hydrogen

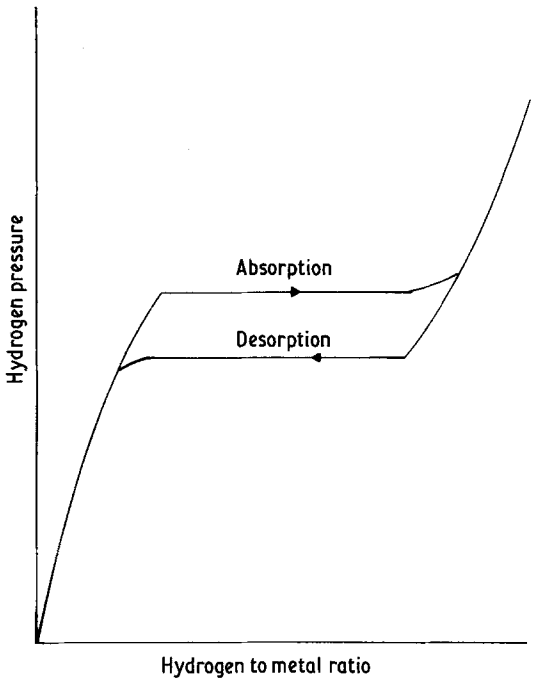

Figure 6 P–C–T diagram showing hysteresis in a metal–hydrogen system [16].

primarily relaxes the residual forces so that the phase is no longer under stress. Therefore, desorption should occur at a lower critical transition pressure. Because of strain sensitivity, the amount and size of impurities as well as processing history have considerable effect on the absorption pressure plateau.

Another explanation for hysteresis is the defect theory by Libowitz *et al.* [31]. This theory assumes that there are non-stoichiometric vacancies in the lattice. As hydrogen is withdrawn from the stoichiometric hydride, hydrogen vacancies are formed, and the hydride becomes non-stoichiometric. At the composition where the lattice becomes saturated with vacancies further removal of hydrogen causes the lattice to break down, thus forming a two-phase system. Therefore, the plateau pressure is actually the equilibrium pressure of non-stoichiometric hydride. On hydriding, it is possible, because of the longer time to reach equilibrium, that a rather stable metastable hydride is formed having fewer vacancies (higher hydrogen composition) than the stable hydride. The metastable hydride, because of the lower stability, has a higher dissociation pressure. Since the hydriding phase has fewer vacancies, the hydriding curve on a P–C–T diagram extends further to the right than the dehydriding curve, as shown in Fig. 6.

Flanagan *et al.* [32] have proposed another approach to hysteresis, based on the solvus behaviour in the palladium–hydrogen system. Large dislocation densities, of the order of $\sim 10^8\,m^{-2}$, are introduced by the $\alpha \rightarrow \beta$ or $\beta \rightarrow \alpha$ phase transitions. The dislocation density in the $\alpha \rightarrow \beta$ followed by the $\beta \rightarrow \alpha$ transformation is about twice that found in the $\beta \rightarrow \alpha$ phase transition. It, therefore, appears that each phase transition leads to its own characteristic dislocation pattern and the contribution due to the reversal of dislocation motion is negligible. In the previous explanations, the desorption isotherm ($\beta \rightarrow \alpha$ transition) was said to approximate the equilibrium condition, whereas Flanagan *et al.* show that neither $P_{\alpha\rightarrow\beta}$ nor $P_{\beta\rightarrow\alpha}$ corresponds to equilibrium, since dislocations, non-equilibrium defects, are generated along each plateau pressure branch.

The degree of hysteresis in a metal–hydrogen system can be affected by the type of testing. Hysteresis is more pronounced in dynamic tests than in conventional static tests [27]. This effect could be due to deformation disordering of the metal lattice by cycling through the high capacity range. An effect of this type has been noted in AB compounds, FeTi [27] and ZrCo [33].

Even though a number of arguments exist on the causes of hysteresis, it is generally agreed that hysteresis reduces the efficiency of hydrogen storage systems.

5. Storage criteria

For hydrides to be useful as energy storage media, a number of requirements are necessary. The hydride should:

(1) be capable of storing large quantities of hydrogen;

(2) be readily formed and decomposed;

(3) be, at least, as safe as other energy carriers;

(4) have reaction kinetics satisfying the charge/discharge requirements of the system;

(5) have the capability of being cycled without alteration in pressure or temperature during the life of the system;

(6) have low hysteresis;

(7) have resistance to poisoning from contaminants such as O_2, H_2O, CO, etc.

(8) have low cost.

A number of materials have been developed but none of them meet all these requirements. The remainder of this report will discuss the major alloy types being studied for energy storage,

namely AB_5, AB, AB_2, Mg-based, and AB_3 and A_2B_7 compounds. The merits and problems associated with each material group will be considered.

6. Metal–hydrogen systems

6.1. AB_5 compounds

The AB_5 compounds, in general, form hydrides with equilibrium pressures of a few atmospheres at temperatures up to 100° C. Other attractive properties are low hysteresis, tolerance to gaseous impurities, and easy activation in the initial cycle. However, most of these compounds contain Ni as the majority metal which makes for a higher cost. The AB_5 family has a hexagonal or orthorhombic structure with the $CaCu_5$-type lattice, as shown in Fig. 7 [34].

The maximum amount of hydrogen that can be absorbed by the AB_5 unit is 9 [34]. There are 12 tetrahedral sites per unit cell; however, 12 hydrogen atoms cannot fit into these sites because of steric interferences. Switendick [35] has shown that the H–H internuclear distance in binary hydrides must be greater than 0.21 nm, but the c-axis in AB_5 compounds is only about 0.4 nm, from $z = 0$ to $z = 1$. Consequently, tetrahedral sites would have to be at positions of $z = 1/4$ and $z = 3/4$, which is not possible without a gross structure change. Therefore, hydrogen atoms cannot occupy both mirror images above and below the $z = 1/2$ plane, leaving a maximum of 6 tetrahedral sites per AB_5 unit. Some of the octahedral sites can degenerate into 4 new sites, as shown in Fig. 7. There are 12 of these sites per unit cell; however, because of steric interferences only 3 of these can be filled. Therefore a total of 9 sites (6 tetrahedral plus 3 octahedral) per AB_5 unit can be filled.

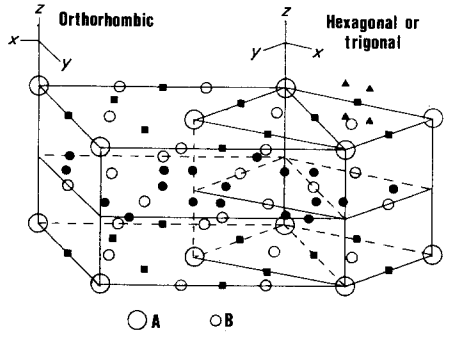

Figure 7 The AB_5 structure shown in both the hexagonal (right) and the orthorhombic (left) lattices. Also shown are tetrahedral (•) and octahedral (▪) hydrogen sites and their possible degeneracies (▲) [34].

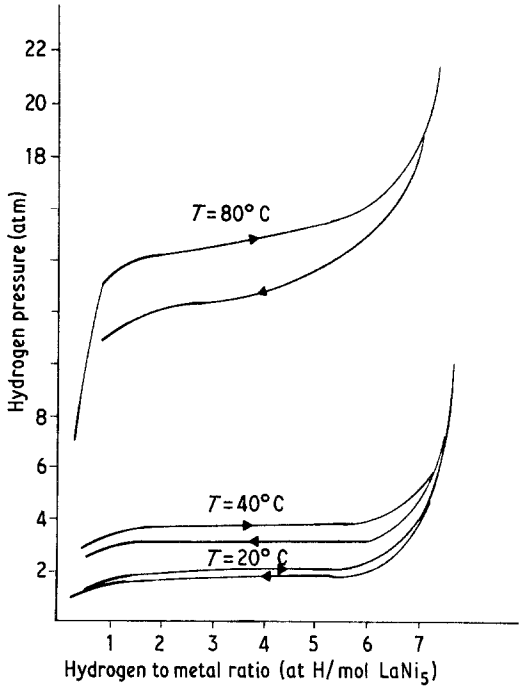

Figure 8 P–C–T plot for the $LaNi_5H$ system [36]. Note that hysteresis is small at low temperatures.

Of the AB_5 intermetallics studied, the one receiving the most attention is the compound $LaNi_5$ which reacts with hydrogen as follows:

$$LaNi_5 + 3H_2 \rightarrow LaNi_5H_6.$$

The pressure–composition isotherm of this material is illustrated in Fig. 8 [36]. From the isotherm, a heat of reaction of ~ -7.2 kcal (mol $H_2)^{-1}$ can be derived with a plateau pressure at room temperature equal to ~ 2.2 atm. The maximum composition that has been reached is $LaNi_5H_{8.35}$ at a hydriding pressure of 1650 atm [34]. The structure of the material remains hexagonal upon hydriding, but there is a lattice expansion of about 25%.

The intermetallic, $LaNi_5$, is characteristic of many hydrogen absorbing compounds, that is, one metal has a strong affinity for hydrogen (La) and the other absorbs little or no hydrogen (Ni) [37]. It is thought that La induces the Ni to become a hydrogen-binding element [36]. Also of interest are the well-known catalytic properties of the nickel surfaces in hydrogenating reactions. In $LaNi_5$ surface segregation occurs [28, 38]. The surface energy is increased by the chemisorption of oxygen, which enhances the segregation effect. Lanthanum diffuses to the surface and bonds with

the oxygen, present in the hydrogen gas as an impurity, to form La_2O_3 or $La(OH)_3$. Nickel, in the surface layer, is no longer the non-magnetic compound $LaNi_5$, but is present in the form of Ni or Ni-rich precipitates. Dissociative chemisorption and associative desorption can occur on the metallic nickel particles or on the metallic subsurfaces of $LaNi_5$. Since the surface segregation and decomposition continue with each cycle, there is continuous formation of fresh Ni particles and of fresh subsurface.

This surface segregation process in $LaNi_5$ is very important in terms of kinetics. Hydrogen absorption in $LaNi_5$ is nearly an order of magnitude faster than FeTi [27] and, in general, AB_5 compounds have better kinetics than AB materials. The hydriding reaction rate is completely controlled by heat transfer. Therefore a good method of heat extraction will enhance absorption kinetics.

Activation or deactivation (poisoning) is also affected by this segregation mechanism. Contaminants in the hydrogen, that is O_2 and H_2O, produce the same effect [39]. There is an initial loss of sorption capacity in O_2 or H_2O containing H_2; however, $LaNi_5$ almost completely recovers and then demonstrates substantial immunity. A fairly thick oxide film forms on the alloy. It appears that complex oxides form initially, with at least part of the surface nickel being oxidized in addition to the expected lanthanum atoms. These complex oxides disproportionate by surface diffusion, resulting in composite films of nickel clusters in a stable oxide or hydroxide (La_2O_2, $La(OH)_3$). This process takes a few hours at room temperature and seems to result in catalytically active nickel. Carbon monoxide, however, is far more detrimental than either oxygen or water vapour. The CO appears to form a simple chemisorbed monolayer, which renders inactive the nickel atom sites at which catalytic dissociation of hydrogen occurs [39]. Reactivation of CO-poisoned samples is partially effective by heating to 80° C and cycling with super-high-purity hydrogen.

Cohen *et al.* [40] found evidence regarding the degradation in sorption properties on cycling. They employed a $LaNi_5$ compound, where some of the La was substituted for Eu, so that Eu could be used as a probe of the hydriding mechanism. Manganese was also substituted for some of the nickel to maintain the plateau pressure, as Eu tended to raise it. The alloy was designated as $LnTM_5$. The amount of hydrogen initially absorbed was about 2.9 mol H_2/mol alloy and it decreased after a period of ~1500 cycles to 0.83 mol H_2/mol alloy, which is only 29% of the original value. Fig. 9 shows the amount of reversibly contained hydrogen in the sample as a function of number of cycles.

Cohen *et al.* observed that the europium was trivalent and metallic in the unhydrided state and divalent in the hydrided phase. After 1500 completed cycles, the Eu was almost entirely in the hydrided divalent state. These results suggested that the reduction in absorption properties was not due to contamination but quite possibly due to the formation of a stable fixed hydride. Results with other compounds, La_2Ni_3 and $EuRh_2$, demonstrated that the smaller the amount of transition metal, the more rapidly the sample was permanently hydrided.

Varying compositions of La–Ni were hydrogenated and examined by Buschow and Van Mal [41], Busch *et al.* [42], and Maeland *et al.* [43]. It was found that as nickel content decreased, the stability of the hydride increased and the amount of hydrogen absorbed increased as well. This is evident, for example in La_2Ni_3 and LaNi which have ΔH values of −36.5 and −25.0 kcal $(mol\,H_2)^{-1}$, respectively, and both compounds absorb up to an H/M ratio of nearly two.

Because of the high cost of $LaNi_5$, some substitution of Ni has been investigated in the hope of reducing the cost. Mendelsohn and Gruen [44] has tried replacing up to 20% of the Ni with Al with dramatic results in lowering decomposition pressures without impairing the kinetics or the

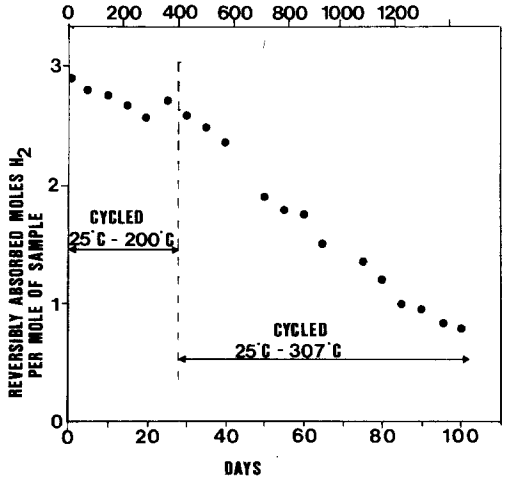

Figure 9 The reversibly absorbed hydrogen as a function of the number of absorption–desorption cycles [40].

hydrogen carrying capacities. As the Al content is increased, the stability of the hydride is increased markedly, i.e., plateau pressures are reduced by up to a factor of 300. Other elements have been substituted for Ni, such as In, Sn, and Ga, and in each case the stability of the hydride was increased without greatly changing the hydrogen to metal ratio [45]. Replacement of 20% of the Ni by Pd, Co, Fe, Cr, Ag, Cu, B [22, 46, 47] lowered the plateau pressure in all cases except for Pd which increased it greatly, as compared to $LaNi_5$. Along with the increased stability comes a subsequent decrease in absorption capacity relative to $LaNi_5$.

Partial substitution of La has also been studied. Van Mal *et al.* [22] have investigated 20% substitutions of La by Nd, Gd, Y, Er, Th, and Zr. In each case, a reduction in stability, i.e., a higher plateau pressure was observed, with approximately the same absorption capacity. Other authors [34, 36] have examined the influence of Ce on $LaNi_5$. The two intermetallics $LaNi_5$ and $CeNi_5$ behave quite differently with respect to hydrogen. $LaNi_5$ absorbs large quantities at relatively low pressures, whereas $CeNi_5$ cannot absorb hydrogen at 150 atm. The addition of Ce does not markedly change the absorption capacity; however, it does raise the plateau pressure substantially. The pressure jump is attributed to the valency change, from + 3 for La to + 4 for Ce.

Other AB_5 compounds of considerable interest are the ACo_5 alloys, where A represents the rare earths. These alloys, unlike the Ni-based compounds, show 3 hydride phases. One of these intermetallics is $LaCo_5$, which has a maximum hydrogen absorption of 9 H atoms/mol $LaCo_5$, with a lower plateau pressure, i.e. below 0.1 atm [34]. The hydrogen capacity is consistent with the prediction of 9 sites (6 tetrahedral and 3 octahedral) per AB_5 units. The majority of the lattice expansion occurs along the *a*-axis, from 0.510 to 0.92 nm. Another ACo_5 alloy of note is $CeCo_5$ [48]. This alloy has a higher plateau pressure than $LaCo_5$ which implies a less stable hydride and a lower critical temperature, T_c. In $CeCo_5$, there is an altered valence state, i.e., from + 3 to + 4, which leads to a small *a*-axis and a small effective cerium radius. Therefore, a higher pressure is required for hydride formation and smaller absorption capacity results, i.e., 7.5 H atoms/mol $CeCo_5$.

In the ACo_5 series, as hydrogen is absorbed, the hydrogen vapour pressure, measured at a given temperature and at a fixed hydrogen to metal ratio, increases with increasing atomic number of A indicating a decreasing affinity for hydrogen as the atomic number is increased [49]. Other AB_5 compounds of interest are listed in Table II along with some of the ones discussed previously for comparison.

6.2. AB compounds

The group of intermetallics, which make up the AB compounds, stores hydrogen at the lowest cost. These materials have equilibrium pressures of a few atmospheres at temperatures up to 100° C.

Most of the work done on AB compounds has been restricted to FeTi. There are two stable intermetallics formed by the Fe–Ti alloy system, FeTi and Fe_2Ti [52]. Fe_2Ti does not absorb appreciable amounts of hydrogen.

The compound FeTi crystallizes in the CsCl-type structure and reacts directly with hydrogen to form an easily decomposed hydride. There are two ternary hydrides formed, i.e., $FeTiH_{\sim 1}$ and $FeTiH_{\sim 2}$ [53]. The solid solution region takes up hydrogen to a composition of $FeTiH_{0.1}$ (α-phase). Once the solubility limit is reached, these two reactions occur:

$$2.13FeTiH_{0.12} + H_2 \rightleftarrows 2.13FeTiH_{1.04}\ (\beta\text{-phase})$$

followed by:

$$2.20FeTi_{1.24} + H_2 \rightleftarrows 2.20FeTiH_{1.95}\ (\gamma\text{-phase}).$$

The pressure–composition isotherms for the FeTi–H system are shown in Fig. 10. The monohydride has a tetragonal structure, while the dihydride forms a cubic structure. The ΔH value for the monohydride is ~ 6.5 kcal $(\text{mol } H_2)^{-1}$.

It is necessary to initially activate FeTi before it will react at a practical rate with hydrogen [54, 55]. This is accomplished by outgassing the alloy at 300° C and contacting it with hydrogen at a pressure of 1 atm.

As in $LaNi_5$ compounds, surface segregation also occurs in FeTi [29, 56–59]. FeTi charged with hydrogen does not remain strongly ordered, but Ti and Fe-clusters are formed in the bulk material. The exchange of metal atom positions necessary for this precipitation occurs near 100° C under the influence of distortion of the lattice caused by dissolved hydrogen. When hydrogen is withdrawn no rearrangement occurs at 100° C. It appears that Ti atoms move to layers close to the surface, while metallic Fe in deeper layers act as a catalyst in the dissociation of hydrogen molecules.

TABLE II Properties of AB_5 hydrides

Compound	Hydride(s)	Hydrogen to metal ratio	Equilibrium plateau pressure* (atm)	ΔH (kcal (mol H_2)$^{-1}$)	Reference
$LaNi_5$	$LaNi_5H_{8.35}$	1.39	2.2	−7.2	[22, 34]
$LaCo_5$	$LaCo_5H_9$	1.5	0.04	−4.5	[22, 34]
$LaFe_5$	$LaFe_5H_6$	1.0	–	−19.0	[22]
$LaCr_5$	$LaCr_5H_6$	1.0	–	−25.0	[22]
$CaNi_5$	$CaNi_5H_6$	1.0	–	−3.0	[22]
$ZrNi_5$	$ZrNi_5H_4$	0.67	–	+9.5	[22]
$ThCo_5$	$ThCo_5H_4$	0.67	–	−5.0	[22]
$ThNi_5$	$ThNi_5H_4$	0.67	–	+3.0	[22]
$ThFe_5$	$ThFe_5H_4$	0.67	–	−12.0	[22]
$LaNi_4Cr$	$LaNi_4CrH_4$	0.67	0.9	–	[22]
$LaNi_4Fe$	$LaNi_4FeH_3$	0.5	1.1	–	[22]
$LaNi_4Co$	$LaNi_4CoH_4$	0.67	1.25	–	[22]
$LaNi_4Cu$	$LaNi_4CuH_{5.7}$	0.95	1.6	–	[22]
$LaNi_4Ag$	$LaNi_4AgH_4$	0.83	2.25	–	[22]
$LaNi_4Pd$	$LaNi_4PdH_{2.5}$	0.42	7.0	–	[22]
$CeCo_5$	$CeCo_5H_{7.5}$	1.25	1.0	–	[22]
$PrCo_5$	$PrCo_5H_6$	1.0	0.8	–	[22]
$LaNi_{4.6}In_{0.4}$	$LaNi_{4.6}In_{0.4}H_5$	0.83	0.054	−9.46	[45]
$LaNi_{4.6}Sn_{0.4}$	$LaNi_{4.6}Sn_{0.4}H_{5.7}$	0.95	0.076	−9.2	[45]
$LaNi_{4.6}Al_{0.4}$	–	–	0.16	−8.7	[45]
$LaNi_{4.6}Ga_{0.4}$	–	–	0.30	−8.4	[45]
$LaNi_4Al$	$LaNi_4AlH_6$	1.0	0.007 (50° C)	−12.7	[44]
$Nd_{0.2}La_{0.8}Ni_5$	$Nd_{0.2}La_{0.8}Ni_5H_6$	1.0	5.5	–	[22]
$Gd_{0.2}La_{0.8}Ni_5$	$Gd_{0.2}La_{0.8}Ni_5H_5$	0.83	9.0	–	[22]
$Y_{0.2}La_{0.8}Ni_5$	$Y_{0.2}La_{0.8}Ni_5H_5$	0.83	10.0	–	[22]
$Er_{0.2}La_{0.8}Ni_5$	$Er_{0.2}La_{0.8}Ni_5H_6$ & $Er_{0.2}La_{0.8}Ni_5H_{3.5}$	1.0	12.0 and 16.0	–	[22]
$SmCo_5$	$SmCo_5H_3$	0.5	3.5	−7.4	[36]
$La_{0.45}Ce_{0.55}Ni_5$	$La_{0.45}Ce_{0.55}Ni_5H_9$	1.5	70	–	[34]
$LaMn_{0.05}Co_{4.95}$	$LaMn_{0.05}Co_{4.95}H_9$	1.5	1.0	–	[34]
$La_{0.5}Ce_{0.5}Co_5$	$La_{0.5}Ce_{0.5}Co_5H_{8.5}$	1.4	0.1	–	[34]
$(La_{0.5}Ce_{0.5})NiCo_{0.5}$	$(La_{0.5}Ce_{0.5})Ni_{4.5}Co_{0.5}H_6$	1.0	15.20	–	[51]
$MNi_{4.5}Cr_{0.5}$‡	$MNi_{4.5}Cr_{0.5}H_{6.3}$	1.05	14 (50° C)	−6.1	[50]
$MNi_{4.5}Mn_{0.5}$‡	$MNi_{4.5}Mn_{0.5}H_{6.6}$	1.1	4 (50° C)	−4.2	[50]
$M_{0.5}Ca_{0.5}Ni_5$‡	$M_{0.5}Ca_{0.5}Ni_5H_5$	0.83	19 (50° C)	−7.6	[50]
$M_{0.3}Ca_{0.7}Ni_5$‡	$Ca_{0.7}M_{0.3}Ni_5H_{5.4}$	0.91	3.8	–	[102]
(CFM)Ni_5†	(CFM)Ni_5H_6	1.0	4.2	–	[102]

*Room temperature unless specified.
†CFM – calcium-free mischmetal.
‡M – mischmetal.

The hydrogen activation process causes the formation of Fe clusters in the vicinity of the surface. From surface studies [28, 57, 59], no trace of iron oxide has been found, which implies that the oxygen is bonded to the Ti atoms. With in-take of hydrogen, the oxide layer is reduced and becomes transparent to hydrogen. Iron precipitates in the deeper layers promote, like a catalyst, the dissociation of the H_2 molecule. The segregation of FeTi on the surface in significant amounts only takes place on heat treatment in a hydrogen atmosphere.

Unlike the AB_5 compounds, the reaction kinetics of the AB compounds, and in particular FeTi, is only partially controlled by heat transfer [27]. Consequently, the chemical reaction rates are of more importance than heat-transfer capability. The reaction procedure, then, is of greater concern. Higher reaction temperatures aid the reaction rate by enhancing the catalytic effect of surface segregation. On the other hand, higher temperatures increase plateau pressures and thus decrease the effective pressure, or the pressure driving force in excess of the equilibrium pressure, slowing down hydride formation [60]. Therefore an optimum reaction temperature is desired. Smaller particle size also tends to increase reaction rates, because of the larger surface area.

The reaction kinetics are severely affected by

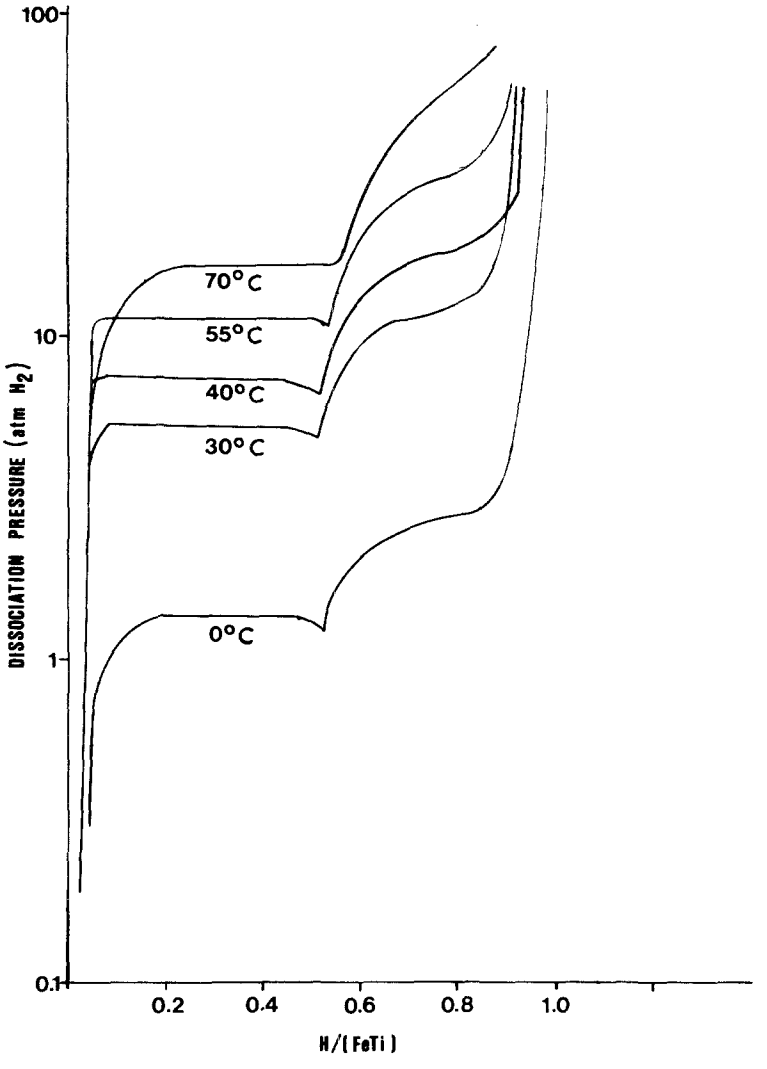

Figure 10 P–C–T plot for the FeTi–H system [52].

contaminants. Poisons, such as O_2, H_2O, and CO, can be very detrimental to the FeTi–H reaction and may even halt the reaction completely [39, 61, 62]. In the presence of O_2 and H_2O, FeTi shows a continuous loss of transfer ability (in terms of H/M ratio) with the number of cycles. The contamination process is essentially the same as in $LaNi_5$, except that a stable titanium oxide forms, (TiO_x). In the FeTi structure, there is no recovery as reported for the $LaNi_5$ compound [39]. The reason for this is unclear; however, it is probable that either the metallic iron is not an $H_2 \rightarrow 2H$ catalytic species in the presence of O_2, or the TiO_x film is impermeable to hydrogen penetration. Carbon monoxide poisoning is characterized by the splitting of CO followed by oxidation and/or carburization of the surface titanium atoms, with the remaining iron bonded by carbonyl radicals [39]. The CO is adsorbed to a thickness of only $\simeq$ one monolayer while O_2 and H_2O are adsorbed to thicknesses of tens of monolayers [39].

Once poisoned, FeTi is difficult to reactivate. In some cases (H_2 and O_2 contamination), recovery can be achieved by cycling with super high-purity H_2 at $\sim 45^\circ$ C. Reactivation of CO contaminated samples is much more difficult. Heating to 80° C and cycling with super-high-purity hydrogen provides some recovery [39].

As is evident in Fig. 11, the FeTi–H system exhibits pronounced hysteresis [52]. It is of note that the system almost forms two loops, since hysteresis is substantially reduced in the intermediate (β) phase region. The loops do not close completely, possibly due to the narrow composition range where only the β-phase is present. Another point of interest is the dip in the desorption isotherm at a hydrogen-to-metal ratio of

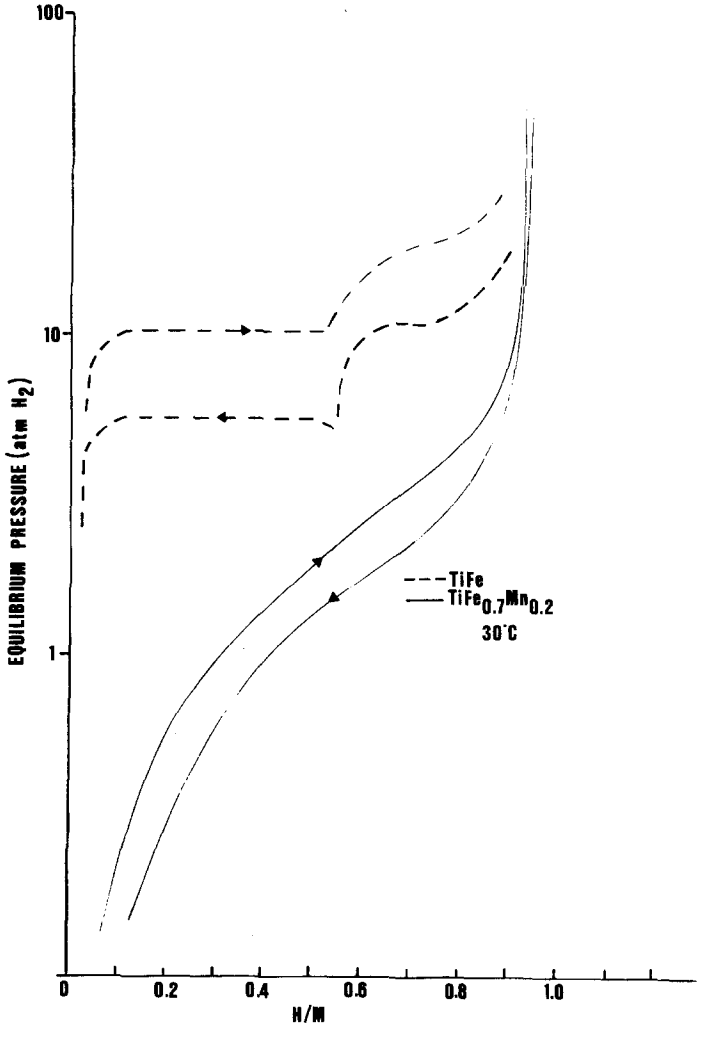

Figure 11 A comparison of the FeTi–H and the $TiFe_{0.7}Mn_{0.2}$–H systems. Note the sloping plateau and the decrease in hysteresis in the $TiFe_{0.7}Mn_{0.2}$–H system [52].

~ 2.5. A possible explanation has to do with the supersaturation of hydrogen vacancies in the hydride phase.

Because of the drawbacks discussed above and the weight of FeTi hydrides, other alloys are being investigated. Ti–Al alloys would be lighter than FeTi, and a Ti–Al alloy could be produced at a cheaper cost [63]. The intermetallic Ti_3Al forms a ternary hydride at room temperature and below. Initially, there is a very rapid sorption, taking only a few minutes, up to a H/M ratio of ~ 2.6. This is followed by a very slow sorption, taking hours or even days, with a maximum uptake of 1.5 H atoms/formula unit. This alloy exhibits two plateaus, corresponding to β and γ hydrides, with a ΔH value of -11.3 kcal. The biggest problem in developing useful Ti–Al–H alloys appears to be the irreversibility of the formation of the γ hydride. To avoid the β-phase, thereby obtaining a wide $\alpha + \gamma$ plateau, would also be desirable.

The addition or substitution of a transition metal in FeTi can distort the P–C–T curves to the point where they are no longer recognizable. In some cases, these distortions can be desirable. The following two points were observed by Reilly [62]:

(1) the addition and/or substitution of another transition metal for iron distorts the pressure–composition isotherm downward as compared to the FeTi–H system;

(2) a wide range of P–C–T characteristics are possible depending upon the third metal component.

The shape of the isotherms of many of these ternary metal alloy–H systems has an appreciable slope, as shown in Fig. 11, indicating exclusive mutual solid solution effects are taking place. Since hysteresis is absent in pure solutions, it can be expected that it would be minimal in these instances. In certain cases where the Ti

concentration is greater than 50 at%, the maximum hydrogen content measurably exceeds that of TiFe–H. The H/M maximum ratio in $TiFe_{0.7}Mn_{0.2}$, for example, slightly exceeds 1.0. Manganese is also attractive in that it is readily available and relatively inexpensive and it has shown some resistance to CO poisoning [39].

Another AB compound of interest is TiCo [64]. This alloy can be activated easily and shows good resistance to impurities. However, the equilibrium dissociation pressure is too low. Manganese can be added to increase the plateau pressure. An alloy of composition $TiCo_{0.5}Mn_{0.5}$ absorbs a maximum of 1.6 wt% hydrogen and has a ΔH value of $-11.2\,\text{kcal}\,(\text{mol}\,H_2)^{-1}$.

Other AB compounds undergoing study are ZrNi [31, 65–67] and ZrCo [68, 69]. Both of these alloys consist of a material that reacts exothermally with large amounts of H_2 (Zr) and a material that absorbs small amounts of hydrogen endothermally (Ni, Co). ZrNi reacts readily with hydrogen to form a brittle powder with a metallic appearance. The maximum amount of hydrogen absorbed at room temperature and 1 atm pressure is ~ 2.94 atoms H/atom Zr. There are believed to be two plateaus, one corresponding to ZrNiH and the other to $ZrNiH_3$. The ΔH value is $-18.4 \pm 0.2\,\text{kcal}\,(\text{mol}\,H_2)^{-1}$. The major drawbacks are the presence of hysteresis and high stability. ZrCo absorbs hydrogen up to a ratio of H/M 1.3. Like ZrNi, the hydride formed is very stable, with a ΔH value of -18.0 to $-19.0\,\text{kcal}\,\text{mol}^{-1}$, and a pronounced hysteresis effect is evident.

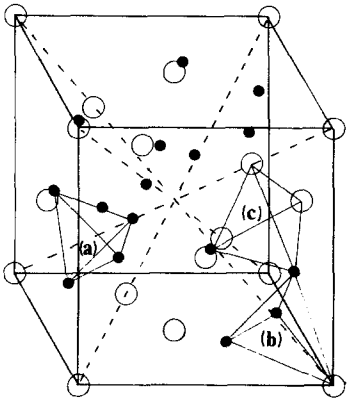

Figure 12 The cubic (C15) Laves phase is shown. The A atoms are shown as open circles and the B atoms as solid ones. The three types of interstitial sites are given; (a) B_4 sites (b) AB_3 sites and (c) A_2B_2 sites [77].

6.3. AB_2 compounds

The AB_2 compounds are probably the most recent of the alloy systems. These materials form hydrides, which have a high storage capacity and resistance to impurities. However, their high thermal stability has resulted in limited technological developments.

The AB_2 compounds form one of two structures, either the cubic C15 structure [70] or the hexagonal C14 structure [71]. These crystal structures are shown in Figs. 12 and 13. Both of these structures are Friauf–Laves phases, belonging to a group of lattice types in which all interstices are formed by tetrahedra [72–77]. As a result, hydrogen absorption increases the size of the unit cell without changing the structure. There are three types of interstitial sites; namely AB_3, A_2B_2 and B_4, where A and B represent the atoms surrounding the site.

Shoemaker and Shoemaker [74] have found the total number of interstitial sites per unit cell to be 17. This number is made up of 4 AB_2 sites, 12 A_2B_2 sites, and 1 B_4 site. However, hydrogen absorption never comes close to a value of 17 hydrogen atoms/formula unit. The primary limiting principle is an electrostatic one. Because hydrogen is more electronegative than the metal atoms, on hydriding the hydrogen atoms become negatively charged. The decreases in enthalpy that accompanies the charge transfer and the resulting

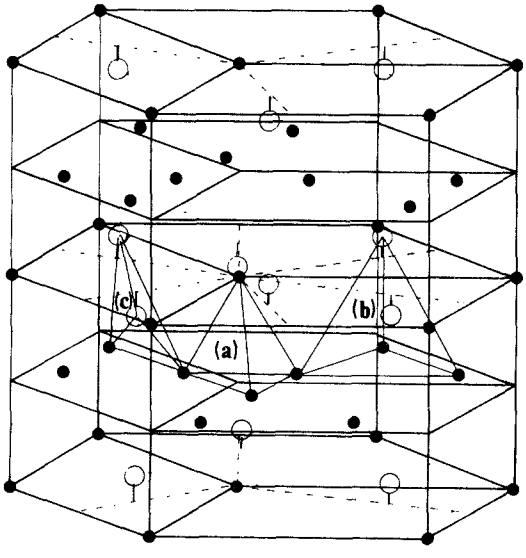

Figure 13 The hexagonal (C14) Laves phase is given. The solid circles represent B atoms and the open circles A atoms. The interstitial sites are shown; (a) B_4 sites, (b) AB_3 sites and (c) A_2B_2 sites [77].

electrostatic interactions are important contributions to the enthalpy of absorption. These must overcome the energy of the H–H molecular bond and the considerable entropy decrease on absorption. Consequently, in a stable hydride, the charged hydrogen atoms cannot occupy positions too close to one another [74]. Shoemaker and Shoemaker [74] have proposed the following exclusion rule: two tetrahedra having a triangular face in common may not both accommodate hydrogen atoms at their centres. By employing this rule, Shoemaker and Shoemaker have deduced a maximum hydrogen occupancy of 6 atoms per formula unit for the C15 structure and $6\frac{1}{3}$ atoms per formula unit for the C14 structure. This calculation is in good agreement with experimental maximum capacities [73, 78–81].

Shaltiel [77] and Didisheim [80] have attempted to determine which interstitial sites are occupied by hydrogen (or deuterium) atoms. Shaltiel [77] has proposed a modified approach to the rule of reversed stability [22, 23]. In order to compare the relative stability of hydrogen atoms in different sites of the metal, a value $\Delta H'$ is assigned to each site, which is the sum of the heats of formation of elementary (imaginary binary) hydrides formed by the surrounding A and B atoms. The heat of formation of these hydrides can be deduced by using the theory of Miedema and co-workers [22, 23], assuming each hydrogen site is equally divided between the surrounding metal atoms (this probably is not true). The hydrogen will preferably occupy interstitial sites with large negative ΔH values.

Didisheim [80] have calculated $\Delta H'$ values for the ZrV_2–D system and the values are plotted against hydrogen (deuterium) concentration in Fig. 14. It is evident that there is a greater tendency for interstices to attract hydrogen as the number of Zr(A) atoms surrounding the site increases. Therefore, the A_2B_2 interstices are occupied first. At a critical concentration x', the $\Delta H'$ values for A_2B_2 and AB_3 holes become equal. At concentrations greater than x', there should be competition between the two sites and both should absorb hydrogen. The B_4 sites have small $\Delta H'$ values and therefore little or no absorption is expected. These predictions are confirmed experimentally (at least qualitatively) by neutron diffraction studies done on the ZrV_2–H system [73, 80].

Shaltiel's model, though it offers good qualitative agreement, neglects some important contributions to stability [80]. One is the weakening of the metal–metal bonds caused by interstitial hydrogen (deuterium) and lattice expansion. This corresponds to the last term of the rule of reversed stability. The second contribution is the electrostatic repulsion of deuterium atoms, and the third is the loss of stability due to a loss in entropy.

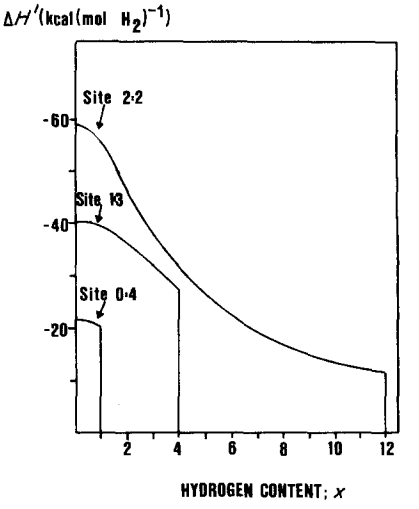

Figure 14 The calculated heats of formation as a function of the hydrogen concentration for the three types of tetrahedral sites in ZrV_2. At the concentration $x \sim 2.5$, the 2-2(A_2B_2) and the 1-3(AB_3) interstices are competitive with respect to hydrogen occupation [75].

There are a number of zirconium-based alloys of the AB_2 classification, that are receiving considerable interest. These alloys have the general formula ZrB_2, where B equals V, Cr, Mn, Fe, Co, or Mo. Hydrogen absorption decreases significantly with an increase in the 3d occupation number of transition elements (B) across the 3d series [78]. The maximum absorption capacity of ZrV_2 is ~ 6 H atoms per formula unit [80, 81] while that of $ZrFe_2$ or $ZrCo_2$ is less than 0.2 H atoms per formula [79]. ZrV_2, which absorbs the most hydrogen of the series, is the only intermetallic in the Zr–V system. There are two phases present in the intermetallic, one hexagonal and the other cubic. Both phases take part about equally in the hydriding process and the basic structure is unchanged. Both Zr_2V_2 and ZrV_3 sites are involved in hydriding, although the more favourable site remains that which presents the higher number of Zr neighbours [81]. $ZrCr_2$, like ZrV_2, absorbs large quantities of hydrogen, approximately 1.3 atoms per formula unit [79, 81]. It also exhibits no hysteresis and has an

extremely low equilibrium pressure at room temperature. $ZrCr_2$ has a C15 cubic structure and some of the cubic phase transforms to the C14 hexagonal hydride, when the absorption limit is approached. The majority of the hydrogen is contained in the Zr_2Cr_2 sites with a small amount in $ZrCr_3$ sites. This could be due to a critical hydrogen concentration (x') being reached at $x' \sim 3.5$, as discussed earlier [80]. The intermetallic, $ZrMo_2$, demonstrates slow absorption and desorption kinetics [79]. The amount of hydrogen absorbed at even low temperatures is only 0.26 atoms H/formula unit. As in the other ZrM_2 compounds, no hysteresis is evident. The other three ZrM_2 intermetallics, i.e., $ZrMn_2$, $ZrFe_2$, and $ZrCo_2$, with the exception of $ZrMn_2$, have hydrogen absorptions that are somewhat lower. The hydrogen absorption in these ZrB_2 compounds can be related to their electron concentrations [79] as shown in Fig. 15. The plot shows that hydrogen dissolution contributes to electron concentration to the extent that phases with lower electron concentration accommodate more hydrogen than those with higher electron concentration. There is other evidence present in the literature that substantiates the claim that electronic factors are more important for AB_2 compounds than structural factors. Both Shaltiel *et al.* [75, 76] and Mendelsohn and Gruen [82] present evidence of this in work done on pseudobinaries with C14 and C15 structures.

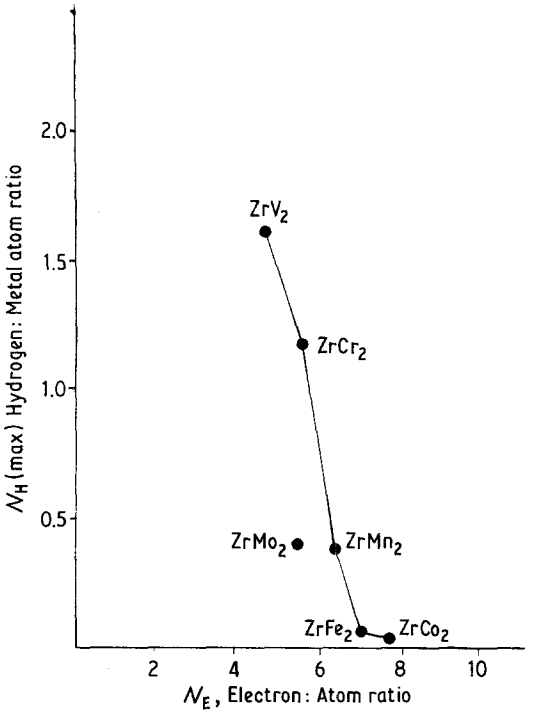

Figure 15 Plot of hydrogen concentration against electron concentration [80].

For the ZrB_2 compounds, a method of raising the equilibrium pressure while maintaining high absorption levels is by the formation of pseudobinary compounds. This was discussed earlier in the section on AB_5 compounds and the mode of action taken is similar here. Substituting some of the V or Cr with Fe or Co decreases the hydrogen capacity some and significantly increases the plateau pressure [66, 75, 78, 82]. Many of the pseudobinary compounds, i.e., $Zr(Co_xM_{1-x})_2$ and $Zr(Fe_xM_{1-x})_2$, form hydrides suitable for storage. Activation is only necessary in a few cases to initiate absorption. For compounds with M=V or Cr, the crystal structure changes, as a function of x, from a cubic C15 structure to hexagonal C14 and back again. For the case where M = Mn, there is a change from hexagonal to cubic. Hydrogen absorption causes a lattice expansion of up to 10% in these alloys and the following observations have been made [75, 78]:

(1) the value of hydrogen capacity decreases as x increases;

(2) compounds containing V show a sharp decrease in hydrogen capacity in the areas $0 \leqslant x \leqslant 0.5$ and $0.85 < x < 1.0$;

(3) compounds containing Mn and Cr do not have the initial sharp decrease as in (2), but there is a sharp decrease for $0.6 < x < 1.0$;

(4) comparing absorption capacity of compounds containing Mn with those containing Cr reveals relatively small differences for values up to $x \sim 0.6$;

(5) pseudobindaries exhibit hysteresis between absorption and desorption isotherms.

Shaltiel and co-workers [75, 77] have developed a phenomenological model to explain absorption capacity in terms of x. They have suggested that absorption capacity is mainly a result of the zirconium local environment, that is nearest neighbours of type A or B for a pseudobinary with the formula ZrA_xB_{1-x}. Shaltiel *et al.* also assume that the crystal structure, i.e., cubic or hexagonal, has no effect on hydrogen absorption since the number (12) and type of nearest and second nearest neighbours are the same and the Zr–A and Zr–B distances are essentially constant. The model is based upon probabilities and can be found in the literature [75, 77, 83]. Good agree-

ment has been observed between experimental data and the theoretical model as evident in Figs. 16 and 17.

Because of the cost and weight of zirconium, some substitution has been investigated. Two such alloys are $Ti_{1-x}Zr_xMn_2$ [76, 84] and $Ti_{1-x}Zr_xCr_2$.

The following observations have been made:

(1) the hydrogen absorption capacity of the $Ti_{1-x}Zr_xCr_2$ system increases linearly with x from 3.3 H atoms/formula unit at $x = 0.0$ to 4.5 H atoms/formula at $x = 1.0$;

(2) hydrogen absorption increases for $(Zr_xTi_{1-x})Mn_2$ from 0.3 H atoms/formula at $x = 0.0$ to 3.65 H atoms/formula at $x = 0.4$; from $0.4 < x < 1.0$, hydrogen absorption is ~4.0 H atoms/formula;

(3) the $(Zr_xTi_{1-x})Cr_2$ hydrides do not release all the hydrogen upon desorption;

(4) the $(Zr_xTi_{1-x})Mn_2$ hydrides release all absorbed hydrogen.

Shaltiel *et al.* [76] attempted to apply a phenomenological model to $(A_xA'_{1-x})B_2$-type pseudo-

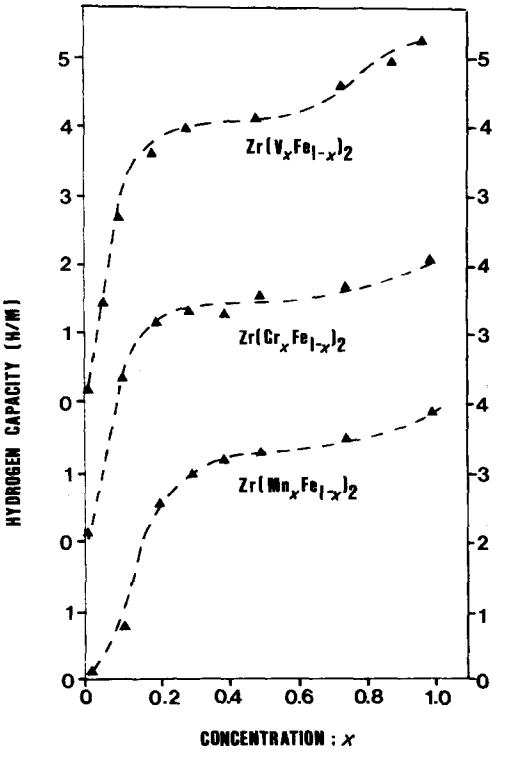

Figure 16 The hydrogen absorption capacity of $Zr(A_xFe_{1-x})_2$ (A = V, Cr, Mn) pseudobinary compounds as a function of the concentration, x. The dashed lines represent the theoretical model [75].

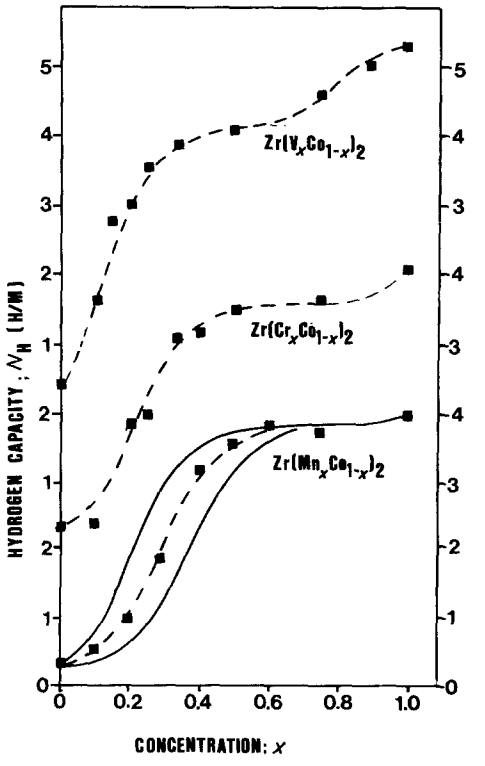

Figure 17 The hydrogen absorption capacity of $Zr(A_xCo_{1-x})_2$ (A = V, Cr, Mn) pseudobinary compounds as a function of the concentration, x. Dashed lines and solid lines represent the theoretical models [75].

binaries in a manner similar to that discussed previously for ZrA_xB_{1-x}. They found that in the $(Zr_xTi_{1-x})Cr_2$ system, absorption was dependent upon nearest neighbours while in the $(Zr_xTi_{1-x})Mn_2$ system, absorption was dependent upon both nearest and second nearest neighbours. Shaltiel *et al.* were unable to explain this discrepancy, but did suggest that the difference in hydrogen affinity between Cr and Mn may have been a factor. A list of various AB_2-type binaries and pseudobinaries are given in Table III along with their corresponding hydrogen absorption properties.

6.4. Mg and Mg-based alloys

Magnesium, as a hydrogen storage material, meets two very important storage criteria. It can store large quantities of hydrogen, much more than twice as much per unit weight than either $LaNi_5$ or FeTi, and it is relatively inexpensive. However, two major obstacles prevent its widespread usage. The Mg–H reaction has poor reaction kinetics and the hydride that is produced is too stable for most practical applications.

TABLE III Hydrides of zirconium binaries and pseudobinaries

Compound	Hydrides	Hydrogen to metal ratio	ΔH (kcal (mol H_2)$^{-1}$)	Equilibrium plateau pressure* (atm)	Reference
$ZrNi_5$	Negligible amounts of hydrogen absorbed				
ZrNi	ZrNiH and $ZrNiH_3$	1.47	−18.4	–	[31]
ZrCo	$ZrCoH_{2.6}$	1.3	−18.0	–	[68]
$TiCr_2$	$TiCr_2H_{3.84}$	1.28	–	1 (−55° C)	[85]
ZrV_2	ZrV_2H_6	2.0	−48.0	10^{-8}	[78, 81]
$ZrCr_2$	$ZrCr_2H_{3.8}$	1.3	−11.0	10^{-8}	[78, 81]
$ZrMn_2$	$ZrMn_2H_{3.6}$	1.2	−12.7	–	[84]
$ZrFe_2$	–	0.2	–	–	[78]
$ZrCo_2$	–	0.2	–	–	[78]
$ZrMo_2$	$ZrMo_2H_{0.78}$	0.26	–	–	[79]
$LaNi_2$	$LaNi_2H_{4.5}$	1.5	–	–	[86]
$La_{2.75}Mg_{0.25}Ni_2$	$La_{2.75}Mg_{0.25}Ni_2H_{4.1}$	1.4	–	–	[86]
$La_{0.4}Mg_{0.6}Ni_2$	$La_{0.4}Mg_{0.6}Ni_2H_{2.9}$	1.0	–	–	[86]
$Ti_{0.6}Zr_{0.4}Mn_2$	$Ti_{0.6}Zr_{0.4}Mn_2H_{0.9}$	0.3	–	20 (140° C)	[84]
$Ti_{0.4}Zr_{0.6}Mn_2$	$Ti_{0.4}Zr_{0.6}Mn_2H_{1.1}$	0.36	–	8.0 (140° C)	[84]
$Ti_{0.2}Zr_{0.8}Mn_2$	$Ti_{0.2}Zr_{0.8}Mn_2H_{1.2}$	0.4	–	1.8 (140° C)	[84]
$Zr(Fe_{0.5}Cr_{0.5})_2$	$Zr(Fe_{0.5}Cr_{0.5})_2H_{3.2}$	1.07	−11.5	0.0012	[78]
$Zr(Fe_{0.75}V_{0.25})_2$	$Zr(Fe_{0.75}V_{0.25})_2H_{3.2}$	1.07	−7.7	0.25	[78]
$Zr(Fe_{0.5}Cr_{0.5})_2$	$Zr(Fe_{0.5}Cr_{0.5})_2H_{3.4}$	1.13	−11.8	0.1	[78]
$Zr(Fe_{0.75}Cr_{0.25})_2$	$Zr(Fe_{0.75}Cr_{0.25})_2H_{2.85}$	0.93	−5.8	5.5	[78]
$Zr(Fe_{0.4}Mn_{0.6})_2$	$Zr(Fe_{0.4}Mn_{0.6})_2H_{3.2}$	1.07	−7.9	0.4	[78]
$Zr(Fe_{0.5}Mn_{0.5})_2$	$Zr(Fe_{0.5}Mn_{0.5})_2H_{2.9}$	0.97	−7.2	0.65	[78]
$Zr(Co_{0.5}V_{0.5})_2$	$Zr(Co_{0.5}V_{0.5})_2H_{3.7}$	1.23	−11.8	0.0023	[78]
$Zr(Co_{0.75}V_{0.25})_2$	$Zr(Co_{0.75}V_{0.25})_2H_{3.0}$	1.0	−8.2	1.5	[78]
$Zr(Co_{0.5}Cr_{0.5})_2$	$Zr(Co_{0.5}Cr_{0.5})_2H_{3.2}$	1.07	−9.6	0.7	[78]
$Zr(Co_{0.25}Mn_{0.75})_2$	$Zr(Co_{0.25}Mn_{0.75})_2H_{3.4}$	1.13	−10.6	0.08	[78]
$Zr(Co_{0.4}Mn_{0.6})_2$	$Zr(Co_{0.4}Mn_{0.6})_2H_{3.1}$	1.03	−8.6	0.5	[78]
$Zr(Co_{0.5}Mn_{0.5})_2$	$Zr(Co_{0.5}Mn_{0.5})_2H_{3.1}$	1.03	−8.3	1.2	[78]

*Given at room temperature unless specified.

Magnesium reacts with hydrogen according to the following reaction:

$$Mg + H_2 \rightleftarrows MgH_2.$$

The amount of hydrogen stored corresponds to 7.6 wt% H and the plateau pressure at 300° C is 1 atm. The slow reaction kinetics are due to the build up of a protective oxide layer on the surface. In an attempt to alleviate these problems, elements such as Cu and Ni have been added to Mg either as alloying additions or catalysts.

The Mg–Cu system forms two intermetallic compounds, namely Mg_2Cu and $MgCu_2$. Only Mg_2Cu reacts readily with hydrogen at reasonable temperatures and pressures. The plateau in the pressure composition isotherm corresponds to the appearance of the reaction [87]:

$$2Mg_2Cu + 3H_2 \rightleftarrows 3MgH_2 + MgCu_2,$$

where the maximum H/M ratio is ~ 1.0. On the right-hand side of the equation, MgH_2 is almost a stoichiometric compound and the dissolution of hydrogen in $MgCu_2$ is negligible. The ΔH value for the reaction is of the order of $\sim -17.4 \pm 1.0$ kcal (mol H_2)$^{-1}$. If Mg is present in the alloy in excess of the composition corresponding to Mg_2Cu, the pressure–composition isotherm exhibits two plateaus. It is believed that the lower plateau is due to the reaction:

$$Mg + H_2 \rightleftarrows MgH_2,$$

and the second plateau is due to the first reaction. The maximum H/M ratio in this case is ~ 1.6. The presence of Mg_2Cu is believed to have a catalytic effect on the Mg–H reaction since substantially higher H_2 pressures and temperatures are needed to form MgH_2 from Mg alone. The heat of formation of MgH_2, assuming that Mg_2Cu acts purely as a catalyst, is -18.7 ± 1.0 kcal (mol H_2)$^{-1}$.

Karty *et al.* [88] have found that the hydriding kinetics of Mg, which is catalysed by Mg_2Cu, is rate-limited by the diffusion of hydrogen through the growing hydride layer and the dehydriding kinetics of Mg, catalysed by Mg_2Cu, is rate-limited by the diffusion of hydrogen through the growing metal layer. This model for hydriding and de-

hydriding kinetics is illustrated schematically in Fig. 18 [88]. The hydrogen enters the Mg not through the Mg external surface, which is easily contaminated, but through the Mg/Mg_2Cu interface which is contamination free. Hydrogen absorption and dissociation occurs at the Mg_2Cu external surface and then the hydrogen diffuses through the Mg_2Cu. Mg_2Cu tends to form low stability oxides, which are reduced and cleaned of oxides by the hydrogen during the hydriding reaction. Seiler [89] offers a variation to this model, implying that Mg_2Cu acts in a manner similar to the surface segregation evident in AB_5 and AB compounds. The Mg diffuses to the surface causing a surface enrichment of Mg. The Mg then forms a very stable oxide with the oxygen while the remaining Cu and underlying matrix is protected. The reason that Mg_2Cu promotes hydrogenation of Mg is because of the absence of a compact oxide layer, as on Mg, and the presence of catalytically active metal clusters and a metallically clean subsurface. According to Viseholm *et al.* [90], the oxide layer only presents a barrier when it is thin and ductile. When the oxide is thick and crystalline, it can crack and allow penetration.

Schlapbach [28] suggested that as long as segregation and decomposition continue, dissociative chemisorption and associative desorption can occur, that is they are not necessarily rate-determining steps. However, as soon as segregation is stopped and the active surface is covered, dissociative chemisorption and associative desorption become rate-determining.

Karty *et al.* [88] have attempted to fit their experimental data for the Mg/Mg_2Cu system to the nucleation and growth equation, previously given in the "kinetics" section. Relatively good fit is obtained in the initial absorption/desorption cycles, but this fit is progressively lost as the number of cycles increases.

Karty *et al.* [88] observed that some of the Mg, in their Mg/Mg_2Cu material, vaporized and then deposited on the reactor wall. This Mg hydrided and dehydrided readily. They interpreted these observations to mean that the H_2 gas was sufficiently clean so that the rate of surface contamination did not keep up with the rate of new Mg surface formation by vapour deposition. The poor fit to the nucleation and growth equation could, thus, be explained by a superposition of reaction kinetics of two different materials. Karty *et al.* utilized the following equation in an attempt to explain their experimental results;

$$f = pf_1 + (1-p)f_2,$$

where p is the fraction of Mg_2Cu-catalysed Mg (bulk material), $1-p$ is the fraction of vapour-deposited Mg, f_1 and f_2 are the growing-phase fractions of catalysed Mg and vapour-deposited Mg, respectively, and f is the total growing fraction. The f_1 and f_2 terms can be calculated using the nucleation and growth equation, where f_1 (or f_2) $= 1 - F(t)$. Good fit was obtained for $p = 70 \pm 5\%$. The values for n are given in Table IV [88].

Another magnesium compound currently under investigation is Mg_2Ni [16, 28, 89–93]. This intermetallic compound reacts with hydrogen to form the ternary hydride Mg_2NiH_4 at temperatures as low as 200° C. Mg_2NiH_4 is believed to form a cubic high-temperature phase which transforms between 245 and 210° C into an orthorhombic low-temperature phase. The ΔH value for the formation of Mg_2NiH_4 is $-15.4\,\text{kcal}\,(\text{mol}\,H_2)^{-1}$. The P–C–T diagram for this system is shown in Fig. 19. As with Mg_2Cu, Mg_2Ni by itself is not of much interest as an energy storage medium. Its primary function is to work as a catalyst for the Mg–H reaction.

The catalytic effect of Mg_2Ni is essentially the same as with Mg_2Cu, except that the Cu atoms are replaced by Ni atoms. The addition of Ni to Mg does not increase the hydriding rate; however, it

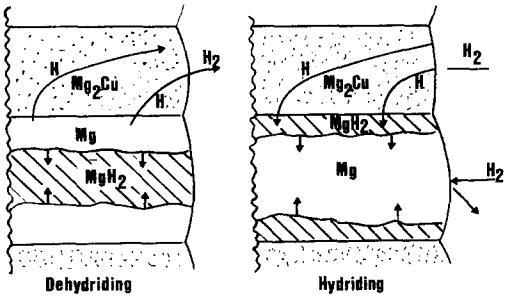

Figure 18 Model of Mg_2Cu-catalysed hydriding and dehydriding of Mg [88].

TABLE IV Experimentally determined μ in Johnson–Mehl–Avrami equation [88]

Mg_2Cu-catalysed Mg		Vapour-deposited Mg	
Hydriding	Dehydriding	Hydriding	Dehydriding
1/2	1	1	2

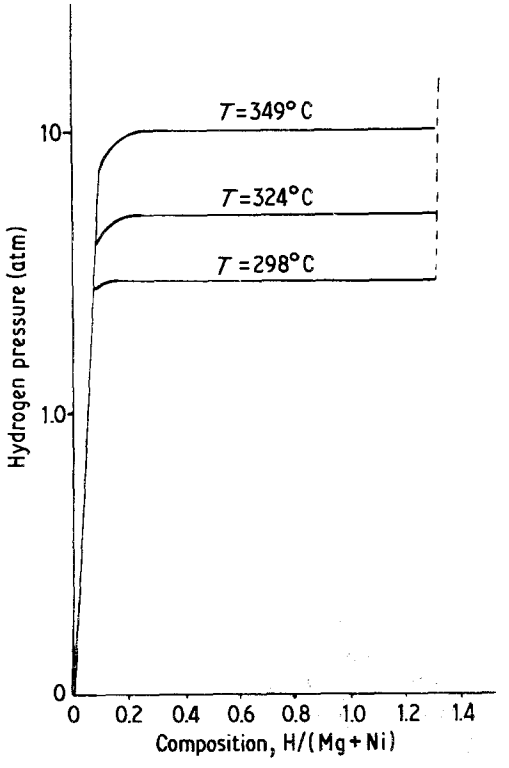

Figure 19 P–C–T plot for the Mg_2Ni–H system [16].

does increase the desorption rate [93, 94]. There is evidence that cycling causes the agglomeration of surface nickel crystallites into larger crystallites, thereby reducing the surface nickel dispersion [94]. This can lead to a reduction in the desorption rate.

Other elements have been added to Mg in efforts to enhance kinetics and/or reduce stability [93, 95]. Additions of rare earths (La, Ce, Mn) improve the reaction kinetics [95], while addition of small amounts of transition metals increase markedly the desorption rates [95]. Mintz [93] has found that the addition of small amounts (< 1 at %) of group IIIa elements enhances the activation process by markedly reducing the activation energy for hydrogenation.

There has been some controversy as to whether the hydrogen anion (H^-) or the Mg cation (Mg^{2+}) is the diffusing species and hence the rate-controlling ion, in the Mg–H reaction [88, 93, 96]. Luz *et al.* [96] have carried out experimental work that may alleviate this problem. Kirkendall marker wires were placed at the Mg surface. After hydriding, the position of the markers was noted. Since the markers appeared to move away from the magnesium metal surface, signifying that the hydride is formed by hydrogen flow past the surface magnesium atoms, hydrogen must be the diffusing species. This model is illustrated schematically in Fig. 20.

6.5. AB_3 and A_2B_7 compounds

Many of the intermetallic compounds, i.e., AB_5, AB_2 and A_2B_7, are closely related structurally [97]. All of these compounds can be derived from the AB_5 structure, see Fig. 21a. The Laves-phases of the form AB_2, as shown in Fig. 21b, are obtained from the AB_5 structure in the following manner. The top layer, in both the AB_2 and AB_5 compound, is the same. The second layer from the top has half the B atoms replaced by A atoms, whereupon the A atoms are then shifted above or below the plane. The third layer is identical to the top layer, except that the atoms are shifted. The continuing stacking sequence determines whether the C14 or C15 structure is obtained. If the fourth

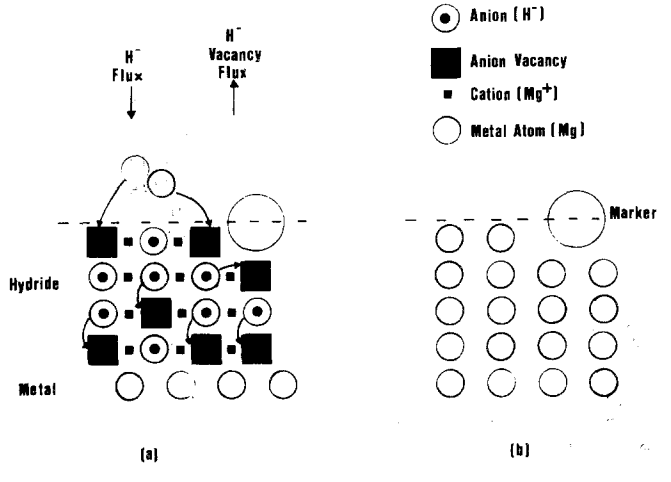

Figure 20 A schematic illustration of the dependence of Kirkedall marker position on the diffusing species upon the hydriding of magnesium; (a) marker position when H anion is the diffusing species, and (b) marker position prior to hydriding [96].

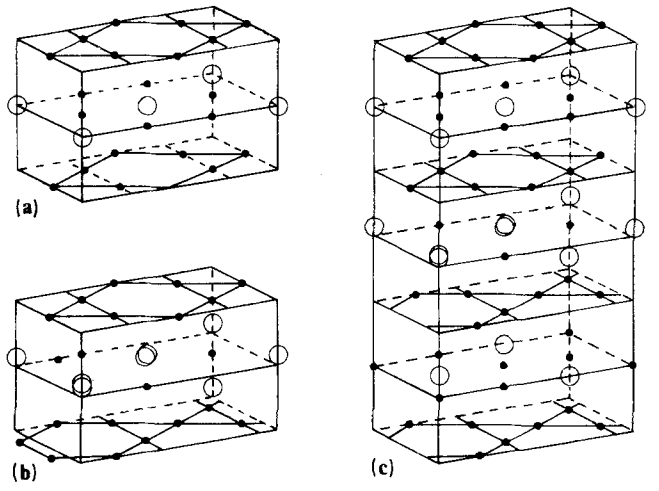

Figure 21 Representative crystal structures for (a) AB_5, (b) AB_2 and (c) AB_3 compounds. Open circles are A atoms and smaller dark circles are B atoms [97].

layer is identical to the second, then the hexagonal $MgCu_2$-type phase is formed. However, if the fourth layer is shifted by the same amount as the third, the cubic $MgCu_2$-type phase is obtained. Since one B atom is converted to an A atom in each AB_5 molecular unit, the following occurs:

$$AB_5 \rightarrow A_2B_4 = 2(AB_2).$$

Other structures are obtained by combining these AB_5 and AB_2 units. By taking one layer of AB_5 with one layer of AB_2, we obtain $AB_5 + 2(AB_2) = 3(AB_3)$, or (see Fig. 21c):

$$AB_3 = \tfrac{1}{3}(AB_5) + \tfrac{2}{3}(AB_2).$$

In the AB_3 structure, one-third of the A atoms have environments that are identical with those of A atoms in the AB_5 compounds and two-thirds of the A atoms have environments like those of A atoms in AB_2 materials. The same approach can be applied to the A_2B_7 compounds. We take two layers of AB_5 plus one layer of AB_2 to yield $2(AB_5) + 2(AB_2) = 2(A_2B_7)$, or:

$$A_2B_7 = AB_5 + AB_2.$$

In this case, half of the A atoms have configurations similar to AB_5 materials, while the other half have environments like those in AB_2 compounds.

TABLE V Properties of selected RT_3 compounds

Compound	Hydrogen to metal ratio	Hydride	Reference	Equilibrium plateau pressure* (atm)
YNi_3	0.3	$YNi_3H_{1.2}$	[98]	0.25
$GdCo_3$	1.08	$GdCo_3H_{4.3}$	[49]	1.0 (175° C)
$TbCo_3$	1.03	$TbCo_3H_{4.1}$	[49]	1.54 (100° C)
$DyCo_3$	1.03	$DyCo_3H_{4.1}$	[49, 99]	–
$HoCo_3$	1.0	$HoCo_3H_{4.0}$	[49]	–
$ErCo_3$	1.0	$ErCo_3H_{4.0}$	[49]	–
$GdFe_3$	0.8	$GdFe_3H_{3.2}$	[49]	1.0 (185° C)
$TbFe_3$	0.9	$TbFe_3H_{3.6}$	[49]	1.0 (180° C)
$DyFe_3$	0.8	$DyFe_3H_{3.2}$	[49]	1.0 (170° C)
$HoFe_3$	0.8	$HoFe_3H_{3.2}$	[49]	1.0 (150° C)
$ErFe_3$	0.7	$ErFe_3H_{2.8}$	[49]	1.0 (140° C)
YFe_3	1.2	$YFe_3H_{4.8}$	[23]	10^{-5}
Th_2Fe_7	0.67	$Th_2Fe_7H_6$	[46]	0.35
$LaNi_3$	1.25	$LaNi_3H_5$	[43]	–
Ce_2Co_7	0.67	$Ce_2Co_7H_6$	[98]	0.5
$CeNi_3$	0.75	$CeNi_3H_3$	[98]	0.09
Y_2Co_7	0.167	$Y_2Co_7H_{1.5}$	[98]	2.5
$PrCo_3$	1.25	$PrCo_3H_5$	[34]	0.1
$ErCo_3$	1.4	$ErCo_3H_{5.5}$	[34]	0.1

*Equilibrium pressure is at room temperature unless specified.

Assuming that there are no long-range H–H interactions, Dunlap *et al.* [97] have predicted the following:

$$n(AB_3) = \tfrac{1}{3}n(AB_5) + \tfrac{2}{3}n(AB_2)$$

and

$$n(A_2B_7) = n(AB_5) + n(AB_2)$$

where $n(A_kB_m)$ represent the hydrogen concentration for each of the respective formula units.

As we have reported previously in this paper, the maximum possible quantity of hydrogen atoms per formula unit in the AB_5 and AB_2 structures is 9 and 6, respectively. Now, if we employ Dunlap's model the following should result:

AB_3: $\frac{1}{3}(9) + \frac{2}{3}(6) = 7$ H atoms/formula unit

A_2B_7: $9 + 6 = 15$ H atoms/formula unit.

In the literature the maximum number of hydrogen atoms reported per AB_3 formula is in the $ErCo_3$–H system. In this case, a composition of $ErCo_3H_{5.5}$ was reached, which does approach the theoretical maximum of 7 [34]. The maximum absorption reported for an A_2B_7 compound is in the Ce_2Ni_7–H system. Here, a composition of $Ce_2N_7H_6$ is realized, which is far below the maximum of 15 [98].

If we consider that in most AB_5 and AB_2 compounds, the maximum absorption reported is approximately AB_5H_6 and AB_2H_4 then the corresponding maximum hydrogen capacities for AB_3 and A_2B_7 compounds is $AB_3H_{4.7}$ and $A_2B_7H_{10}$. A number of AB_3 alloys approach or reach this composition, namely $PrCo_3(PrCo_3H_5)$, $ErCo_3(ErCo_3H_{5.5})$, $CeCo_3(CeCo_3H_4)$, and $DyCo_3(DyCo_3H_{4.25})$ [34, 98, 99]. None of the A_2B_7 compounds approach the value of 10. However, considerably more research needs to be done on these alloys before the Dunlap model is either adopted or discarded.

The AB_3 compounds, in general, form hydrides that are quite stable and they exhibit little or no hysteresis [49]. The A_2B_7 compounds are generally quite stable as well, though slightly less stable than their AB_3 counterparts. This phenomenon may be explained qualitatively by Dunlap's model. AB_2 hydrides are generally much more stable than AB_5 hydrides (the stability of AB_3 and A_2B_7 hydrides lies in between). The A_2B_7 compound has a larger percentage of the AB_5 structure than the AB_3 compound (50% as against 33%). Therefore, more AB_5 hydrides will form in A_2B_7 materials, lowering the overall stability. A list of various AB_3 and AB_7 hydrides is given in Table V.

7. Miscellaneous hydriding materials

A number of materials, which can be classified as A_2B compounds have demonstrated good hydrogen absorption. These intermetallics are Zr_2Cu, Hf_2Cu and Ti_2Cu.

The crystal structure of $CuZr_2$ is tetragonal and of $MoSi_2$-type [100]. This alloy belongs to the group of intermetallics which decompose under the influence of hydrogen to form binary hydrides of the more reactive metallic component. The β-phase region is homogeneous and is denoted as a ternary hydride of the starting phase $CuZr_2$, i.e., $CuZr_2H_{2.88}$. The α-phase consists of decomposition products of the original, i.e., zirconium hydride, and an unidentified new compound which is richer in copper than $CuZr_2$.

The compound Ti_2Cu also decomposes when reacted with hydrogen [100]:

$$Ti_2Cu + 2H_2 \xrightarrow[0.13\ \text{atm}]{200^\circ\ \text{C}} 2TiH_2 + Cu.$$

At temperatures less than 200° C, an intermetallic hydride phase, $Ti_2CuH_{\sim 2.8}$ has been reported. Hf_2Cu forms an intermetallic hydride phase, $Hf_2CuH_{2.9}$, when reacted with hydrogen at 50° C [100].

A relatively new group of materials, in terms of hydrogen storage, is the metallic glasses. Maeland *et al.* [101] have done some work on the Ti–Cu glass system. In both TiCu and $Ti_{0.65}Cu_{0.35}$ they have observed larger hydrogen absorption capacities than in their crystalline counterparts. The glass, $Ti_{0.65}Cu_{0.35}$, for example, can absorb 35% more hydrogen than the corresponding crystalline compound. These results demonstrate the importance of electronic structure and crystal structure in hydrogen absorption. It appears that the maximum absorption capacity is determined by the electronic structure, which is quite similar in the glass and the corresponding intermetallic. However, the crystal structure, i.e., the type and size of the interstitial sites in the lattice, may not always allow maximum absorption to occur.

8. Comparison of hydriding materials

The five alloy glasses, that have been discussed, are compared with one another in Table VI. As one can see, from the table, no one alloy meets all the storage requirements. However, a number of the problems are being reduced or eliminated by alloy substitution. Examples of this are evident in the AB and AB_2 compounds. Manganese additions to

TABLE VI Summary of hydriding alloys and their properties

Alloy type	Quantity of hydrogen absorbed		Kinetics	Stability of hydride
	H/M	wt%		
AB_5, e.g., $LaNi_5$, $LaCo_5$, $CeCo_5$, $LaMn_xCo_{5-x}$	1.0 up to 1.5	1.4% to max 1.9%	Rapid kinetics, of the order of a few seconds due to surface segregation. Heat-transfer controlled. No activation required.	Relatively stable. $\Delta H - 7$ kcal mol^{-1}, ± 3 kcal mol^{-1}. Stability changes, up or down, with alloy substitutions. $P_{eq} \sim 2.2$ atm at r.t. for $LaNi_5$.
AB, e.g., FeTi, ZrNi, TiAl, $Fe_{1-x}Mn_xTi$	1.0	1.8% max	Moderate kinetics partially controlled by heat transfer. Needs activation for surface segregation.	Stability varies from $\Delta H - 7.0$ kcal mol^{-1} for FeTi based alloys to $\Delta H = -11.0$ to -19.0 kcal mol^{-1} for other AB compounds. P_{eq} 4 to 5 atm at R.T.
AB_2, e.g., ZrV_2, $ZrCr_2$, $ZrMn_2$, $LaNi_2$, $Zr(Fe_xV_{1-x})_2$, $Zr(Co_xCr_{1-x})_2$	From 1.0 up to 2.0	From 1.5 to 2.0%	Rapid kinetics. No activation necessary in most cases. Not much data on kinetics, however.	Generally quite stable. $\Delta H - 18.0$ kcal mol^{-1} for binaries. Pseudo-binaries decrease stability to acceptable levels.
Mg-compounds, e.g., Mg, Mg_2Ni, Mg_2Cu	1.3 up to 2.0	From 3.5% up to 6.7%	Sluggish kinetics. Activation is necessary and difficult. Rate limited by diffusion of H atoms (when activated). If segregation stops rate limited by dissociative chemisorption and associative desorption. Ni, Cu, etc. are added as catalysts.	Very stable. $\Delta H \sim -18.0$ kcal mol^{-1}. $P_{eq} \sim 1$ atm at 300° C.
$AB_3 + A_2B_7$, e.g., $ErCo_3$, VFe_3, $CeCo_7$, Th_2Fe_7	Max of 1.4 for AB_3. Max of 0.67 for A_2B_7.	Max of 1.6% Generally much less though.	Not reported.	Quite stable. AB_3 compounds are more stable than A_2B_7 compounds.

Cycling degradation	Hysteresis	Resistance to poisoning	Cost
May be degradation after 300–400 cycles due to formation of stable hydrides ($LaNi_5$).	Moderate hysteresis at low temperatures.	Good resistance to H_2O and O_2 poisoning. Susceptible to CO poisoning, partial reactivation possible.	Quite expensive because of cost of La and Ni.
No evidence as yet, but no high cycle experiments have been done.	Pronounced hysteresis in FeTi; however, can be reduced by addition of Mn.	General poor resistance to poisoning for FeTi. Especially susceptible to CO. Partial reactivation possible. Addition of Mn gives better Co resistance.	Relatively inexpensive. Fe fairly cheap.
No evidence as yet, but no high cycle experiments have been done.	Low hysteresis in binary compounds. Moderate hysteresis in pseudobinaries.	No reported poisoning problems, but little work has been done in this area.	Quite expensive because of cost of Zr metal.
Cycling may cause reduction in desorption rate of $Mg–Mg_2Ni$.	None reported.	Very susceptible to poisoning by O_2, H_2O, CO, etc.	Relatively inexpensive because of high Mg content.
Not reported.	Little or no hysteresis.	Not reported.	Not too expensive since Co and Fe are majority metals in most cases.

FeTi have decreased hysteresis and contamination problems, while iron and cobalt additions to ZrB_2 (B = V, Cr, Mn) materials have reduced stabilities to practical levels. A better understanding of surface processes, i.e., segregation, contamination, chemisorption, etc., will result in more efficient hydrogen storage materials.

References

1. R. L. LEROY, *Canadian Metall. Q.* **17** (1978) 1.
2. C. E. BAMBERGER and J. H. DEVAN, *Metall. Trans.* **9A** (1978) 201.
3. D. P. GREGORY and J. B. PANGBORN, "Hydrogen Fuel Technology Session", Chicago, April and May 1974, (PSC, Red Bank, New Jersey, 1974) p. 1.
4. DAVID A. MATHIS, "Hydrogen Technology For Energy" (New Jersey, USA, 1976).
5. F. J. EDESKUTY and K. D. WILLIAMSON Jr., *Hydrogen* **2** (1977) 51.
6. J. TOEPLER, O. BERNAUER and H. BUCHNER, *J. Less-Common Metals* **74** (1980) 385.
7. C. FOLONARI, G. IEMMI, F. MANFREDI and A. ROLLE, *ibid.* **74** (1980) 371.
8. G. L. HOLLECK, J. R. DRISCOLL and B. E. PAUL, *ibid.* **74** (1980) 379.
9. KEI NOMURA and YOSHIHIKO ISHIDO, *Energy Conversion* **19** (1979) 49.
10. G. G. LIBOWITZ and Z. BLANK, *Solid State Chem.* **19** (1977) 271.
11. F. E. LYNCH, *J. Less-Common Metals* **74** (1980) 411.
12. J. H. SWISHER, *ibid.* **74** (1980) 301.
13. J. HORD and W. R. PARRISH, *Hydrogen* **5** (1979) 3.
14. D. G. WESTLAKE, C. B. SATTERWRITE and J. H. WEAVER, *Physics Today* (November) (1978) 32.
15. G. R. PIERCY, *Canadian Metall. Q.* **17** (1978) 11.
16. J. J. REILLY, *Hydrogen* **2** (1977) 13.
17. A. C. SWITENDICK, *Solid State Commun.* **8** (1970) 1463.
18. J. H. WEAVER and D. T. PETERSON, *J. Less-Common Metals* **74** (1980) 207.
19. J. W. WARD, *ibid.* **73** (1980) 183.
20. H. BUCHNER, *Int. J. Hydrogen Energy* **3** (1978) 385.
21. TED B. FLANAGAN, *J. Phys. Chem.* **79** (1975) 444.
22. H. H. VAN MAL, K. H. J. BUSCHOW and A. R. MIEDEMA, *J. Less-Common Metals* **35** (1974) 65.
23. A. R. MIEDEMA, K. H. J. BUSCHOW and H. H. VAN MAL, *ibid.* **49** (1976) 473.
24. D. M. GRUEN and M. MENDELSOHN, *ibid.* **55** (1977) 149.
25. J. W. LARSEN and B. R. LIVESAY, *ibid.* **73** (1980) 79.
26. S. SUDA, N. KOBAYASHI and K. YOSHIDA, *ibid.* **73** (1980) 119.
27. P. D. GOODELL, G. D. SANDROCK and E. L. HUSTON, *ibid.* **73** (1980) 135.
28. L. SCHLAPBACH, *ibid.* **73** (1980) 145.
29. F. A. KUIJPERS and H. H. VAN MAL, *ibid.* **23** (1971) 395.
30. C. E. LUNDIN and F. E. LYNCH in "Hydrides for Energy Storage" (Pergamon Press, Elmsford, New York, 1977) p. 395.
31. G. G. LIBOWITZ, H. F. HAYES and T. R. P. GIBB, *Inorg. Chem.* **62** (1957) 76.
32. TED B. FLANAGAN, B. S. BOWERMAN and G. E. BIEHL, *Scripta Metall.* **14** (1980) 443.
33. S. J. C. IRVINE and I. C. HARRIS in "Hydrides for Energy Storage" (Pergamon Press, Elmsford, New York, 1977) p. 431.
34. J. F. LAKNER, F. S. URIBE and S. A. STEWARD, *J. Less-Common Metals* **72** (1980) 87.
35. A. C. SWITENDICK, Theoretical Studies of Hydrogen in Metals: Current Status and Further Prospects, Sandia Laboratories, Albuquerque, New Mexico, SAND 78-0250 (1978).
36. J. H. N. VAN VUCHT, *Phillips Res. Rep.* **25** (1970) 133.
37. S. W. STAFFORD, *Acta Metall.* **22** (1974) 1463.
38. L. SCHLAPBACH, *Int. J. Hydrogen Energy* **4** (1979) 21.
39. G. D. SANDROCK and P. D. GOODELL, *J. Less-Common Metals* **73** (1980) 161.
40. R. L. COHEN, K. W. WEST and J. H. WERNICK, *ibid.* **70** (1980) 229.
41. K. H. J. BUSCHOW and H. H. VAN MAL, *ibid.* **29** (1972) 203.
42. G. BUSCH, L. SCHLAPBACH and T. VON WALDKIRCH, *ibid.* **60** (1978) 83.
43. A. J. MAELAND, A. F. ANDRESEN and K. VIDEM, *ibid.* **45** (1976) 347.
44. M. H. MENDELSOHN and D. M. GRUEN, *Nature* **269** (1977) 45.
45. M. H. MENDELSOHN, D. M. GRUEN and A. E. DWIGHT, *Mater. Res. Bull.* **13** (1978) 1221.
46. K. H. J. BUSCHOW, *J. Less-Common Metals* **42** (1975) 163.
47. M. H. MENDELSOHN, D. M. GRUEN and G. D. SANDROCK, *ibid.* **70** (1980) 273.
48. HENRY A. KIERSTEAD, *ibid.* **71** (1980) 311.
49. C. A. BECHMAN, *Inorg. Chem.* **15** (1976) 2185.
50. Y. OSUMI, *J. Less-Common Metals* **74** (1980) 271.
51. D. DAYAN, M. H. MINTY and M. P. DARIEL, *J. Less-Common Metals* **73** (1980) 15.
52. J. J. REILLY, *Inorg. Chem.* **13** (1974) 218.
53. R. C. BOWMAN, *Int. J. Hydrogen Energy* **2** (1977) 309.
54. S. STRICKLAND, *ibid.* **2** (1977) 309.
55. D. L. HENRIKSEN, D. B. MACKAY and V. R. ANDERSON, in "1st World Hydrogen Energy Conference", Vol. 7C, Florida, March 1976, (University of Miami, Miami, 1977) p. 1.
56. G. BUSCH, *Int. J. Hydrogen Energy* **4** (1979) 29.
57. A. BLASIUS and U. GONSER, *Appl. Phys.* **22** (1980) 331.
58. D. FRUCHART, *J. Less-Common Metals* **74** (1980) 55.
59. G. K. SHENOY, *ibid.* **73** (1980) 171.
60. D. G. JOHNSON and J. B. PANGBORN, *ibid.* **73** (1980) 127.
61. P. FISCHER, *Mater. Res. Bull.* **13** (1978) 931.
62. J. J. REILLY, in "1st World Hydrogen Energy Con-

ference", Vol. 2C, Florida, March 1976, (University of Miami, Miami, 1976) p. 29.
63. P. S. RUDMAN, *J. Less-Common Metals* **58** (1978) 231.
64. Y. OSUMI, *ibid.* **72** (1980) 79.
65. JEAN-LOUIS BARON, *J. Nucl. Mater.* **83** (1979) 286.
66. R. WISWALL, *Hydrogen in Metals 11* **29** (1978) 201.
67. D. G. WESTLAKE, *J. Less-Common Metals* **75** (1980) 177.
68. R. M. VAN ESSEN, *ibid.* **64** (1979) 277.
69. S. J. C. IRVINE and I. R. HARRIS, *ibid.* **74** (1980) 33.
70. J. B. FRIAUF, *J. Amer. Chem. Soc.* **49** (1927) 3107.
71. J. B. FRIAUF, *Phys. Rev.* **29** (1927) 34.
72. CHARLES B. MAGEE, *J. Less-Common Metals* **78** (1981) 119.
73. D. SHALTIEL, *ibid.* **73** (1980) 329.
74. D. P. SHOEMAKER and C. B. SHOEMAKER, *ibid.* **68** (1979) 43.
75. I. JACOB, *Solid State Commun.* **23** (1977) 669.
76. *Idem, J. Less-Common Metals* **73** (1980) 369.
77. D. SHALTIEL, *ibid.* **62** (1978) 407.
78. *Idem, ibid.* **53** (1977) 117.
79. A. PEBLER and E. A. GULBRANSEN, *Trans. AIME* **239** (1967) 1593.
80. J. J. DIDISHEIM, *J. Less-Common Metals* **73** (1980) 355.
81. D. FRUCHART, *ibid.* **73** (1980) 363.
82. M. H. MENDELSOHN and D. M. GRUEN, *ibid.* **78** (1981) 275.
83. HENRY A. KIERSTEAD, *ibid.* **70** (1980) 285.
84. H. OESTERREICHER, *Mater. Res. Bull.* **13** (1978) 83.
85. J. R. JOHNSON, *J. Less-Common Metals* **73** (1980) 345.
86. H. OESTERREICHER and H. BITTNER, *ibid.* **73** (1980) 339.
87. J. J. REILLY and R. WISWALL, *Inorg. Chem.* **6** (1967) 2220.
88. A. KARTY, J. GRUNZWEIG-GENOSSAR and P. S. RUDMAN, *J. Appl. Phys.* **50** (1979) 7200.
89. A. SEILER, *J. Less-Common Metals* **73** (1980) 193.
90. B. VIZEHOLM, J. KJOLLER and B. LARSEN, *ibid.* **74** (1980) 341.
91. D. L. DOUGLASS, *Met. Trans.* **6A** (1975) 2179.
92. J. SCHEFER, *J. Less-Common Metals* **74** (1980) 65.
93. M. H. MINTZ, *ibid.* **74** (1980) 263.
94. F. G. EISENBERG, D. A. ZAGNOLI and J. J. SHERIDAN III, *ibid.* **74** (1980) 323.
95. M. PEZAT, B. DARRIET and P. HAGENMULLER, *ibid.* **74** (1980) 427.
96. Z. LUZ, J. SENOSSAR and P. S. RUDMAN, *ibid.* **73** (1980) 113.
97. B. D. DUNLAP, P. J. VICCARO and G. K. SHENOY, *ibid.* **74** (1980) 75.
98. R. H. VAN ESSEN and K. H. J. BUSCHOW, *ibid.* **70** (1980) 189.
99. HENRY A. KIERSTEAD, *ibid.* **73** (1980) 61.
100. R. KADEL and A. WEISS, *ibid.* **65** (1979) 89.
101. A. J. MAELAND, L. E. TANNER and G. G. LIBOWITZ, "Hydrides For Energy Storage" (Pergamon Press, Elmsford, New York, 1978) p. 447.
102. G. D. SANDROCK, *Alternative Energy Sources* **8** (1978) 3713.

Received 1 June
and accepted 21 June 1982